

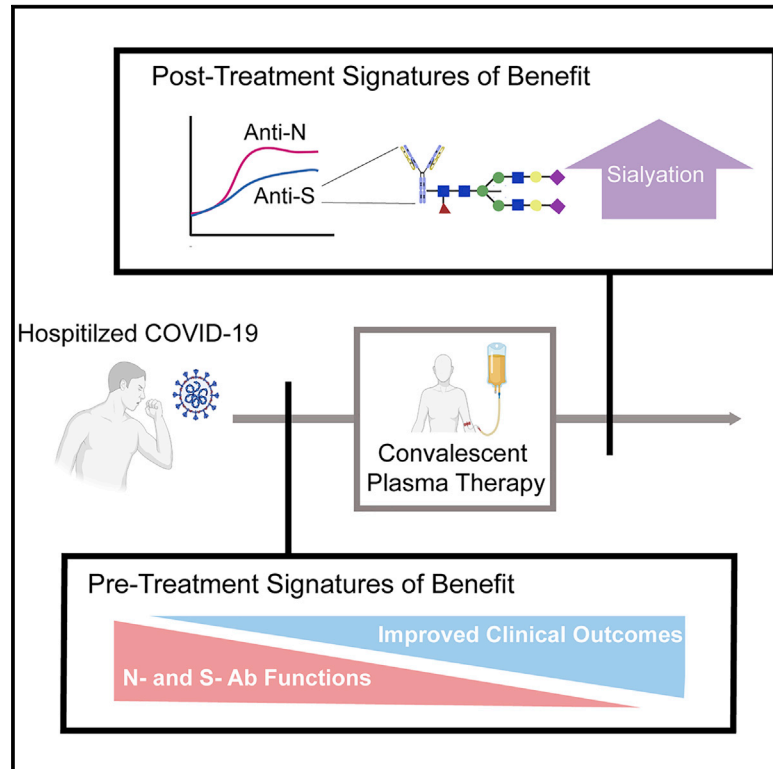


Since January 2020 Elsevier has created a COVID-19 resource centre with free information in English and Mandarin on the novel coronavirus COVID-19. The COVID-19 resource centre is hosted on Elsevier Connect, the company's public news and information website.

Elsevier hereby grants permission to make all its COVID-19-related research that is available on the COVID-19 resource centre - including this research content - immediately available in PubMed Central and other publicly funded repositories, such as the WHO COVID database with rights for unrestricted research re-use and analyses in any form or by any means with acknowledgement of the original source. These permissions are granted for free by Elsevier for as long as the COVID-19 resource centre remains active.

# Nucleocapsid-specific antibody function is associated with therapeutic benefits from COVID-19 convalescent plasma therapy

## Graphical abstract



## Authors

Jonathan D. Herman, Chuangqi Wang, John Stephen Burke, ..., Katharine J. Bar, Douglas Lauffenburger, Galit Alter

## Correspondence

bark@pennmedicine.upenn.edu (K.J.B.), lauffen@mit.edu (D.L.), galter@mgh.harvard.edu (G.A.)

## In brief

Viral neutralization is presumed to be essential for the activity of COVID-19 convalescent plasma (CCP). Herman et al. use high-dimension antibody profiling to interrogate the effects of CCP on the recipient's humoral immune response and how its modulation could affect COVID-19 clinical outcomes.

## Highlights

- Clinical benefits of CCP are associated with a shift in recipient humoral profiles
- Nucleocapsid (N)-specific responses are enhanced in CCP recipients
- CCP most benefits recipients with low pre-existing anti-COVID antibody function
- CCP-associated titer and Fc glycan changes persist for 2 months



## Article

# Nucleocapsid-specific antibody function is associated with therapeutic benefits from COVID-19 convalescent plasma therapy

Jonathan D. Herman,<sup>1,2,10</sup> Chuangqi Wang,<sup>3,10</sup> John Stephen Burke,<sup>1</sup> Yonatan Zur,<sup>1</sup> Hacheming Compere,<sup>1</sup> Jaewon Kang,<sup>1</sup> Ryan Macvicar,<sup>1</sup> Sabian Taylor,<sup>1</sup> Sally Shin,<sup>1</sup> Ian Frank,<sup>4</sup> Don Siegel,<sup>5</sup> Pablo Tebas,<sup>4</sup> Grace H. Choi,<sup>6</sup> Pamela A. Shaw,<sup>7</sup> Hyunah Yoon,<sup>8</sup> Liise-anne Pirofski,<sup>8,9</sup> Boris D. Julg,<sup>1</sup> Katharine J. Bar,<sup>4,\*</sup> Douglas Lauffenburger,<sup>3,\*</sup> and Galit Alter<sup>1,11,\*</sup>

<sup>1</sup>Ragon Institute of MGH, MIT, and Harvard, Cambridge, MA, USA

<sup>2</sup>Division of Infectious Disease, Brigham and Women's Hospital, Boston, MA, USA

<sup>3</sup>Department of Biological Engineering, Massachusetts Institute of Technology, Cambridge, MA, USA

<sup>4</sup>Department of Medicine, University of Pennsylvania, Philadelphia, PA, USA

<sup>5</sup>Department of Pathology and Laboratory Medicine, University of Pennsylvania, Philadelphia, PA, USA

<sup>6</sup>Department of Biostatistics, Epidemiology, and Informatics, University of Pennsylvania, Philadelphia, PA, USA

<sup>7</sup>Biostatistics Unit, Kaiser Permanente Washington Health Research Institute, Seattle, WA, USA

<sup>8</sup>Division of Infectious Diseases, Department of Medicine, Albert Einstein College of Medicine and Montefiore Medical Center, Bronx, NY, USA

<sup>9</sup>Department of Microbiology and Immunology, Albert Einstein College of Medicine, Bronx, NY, USA

<sup>10</sup>These authors contributed equally

<sup>11</sup>Lead contact

\*Correspondence: [bark@penmedicine.upenn.edu](mailto:bark@penmedicine.upenn.edu) (K.J.B.), [lauffen@mit.edu](mailto:lauffen@mit.edu) (D.L.), [galter@mgh.harvard.edu](mailto:galter@mgh.harvard.edu) (G.A.)

<https://doi.org/10.1016/j.xcrm.2022.100811>

## SUMMARY

Coronavirus disease 2019 (COVID-19) convalescent plasma (CCP), a passive polyclonal antibody therapeutic agent, has had mixed clinical results. Although antibody neutralization is the predominant approach to benchmarking CCP efficacy, CCP may also influence the evolution of the endogenous antibody response. Using systems serology to comprehensively profile severe acute respiratory syndrome coronavirus 2 (SARS-CoV-2) functional antibodies of hospitalized people with COVID-19 enrolled in a randomized controlled trial of CCP (ClinicalTrials.gov: NCT04397757), we find that the clinical benefits of CCP are associated with a shift toward reduced inflammatory Spike (S) responses and enhanced nucleocapsid (N) humoral responses. We find that CCP has the greatest clinical benefit in participants with low pre-existing anti-SARS-CoV-2 antibody function and that CCP-induced immunomodulatory Fc glycan profiles and N immunodominant profiles persist for at least 2 months. We highlight a potential mechanism of action of CCP associated with durable immunomodulation, outline optimal patient characteristics for CCP treatment, and provide guidance for development of a different class of COVID-19 hyperinflammation-targeting antibody therapeutic agents.

## INTRODUCTION

The coronavirus disease 2019 (COVID-19) pandemic has claimed more than 4.5 million lives to date.<sup>1</sup> Despite the development and deployment of vaccines to prevent severe COVID-19 and hospitalization, a significant portion of the world's population still remains unvaccinated. The evolution of severe acute respiratory syndrome coronavirus 2 (SARS-CoV-2) variants of concern that are more infectious and more evasive of prior immunity fuels an urgent need for more effective therapeutic agents for hospitalized individuals with severe COVID-19.

Because of its immediate availability and safety profile, COVID-19 convalescent plasma (CCP) was one of the first treatments for COVID-19.<sup>2</sup> However, evidence of CCP clinical efficacy has been mixed. Smaller clinical trials have shown a benefit

of high-titer CCP in patients early in the course of COVID-19.<sup>3–9</sup> However, larger trials have not found an overall benefit of CCP, with the caveat that many of these trials treated patients with severe COVID-19 at later stages of disease.<sup>10,11</sup> Along these lines, the CONCOR-1 trial, a large, randomized controlled trial of CCP in hospitalized patients with COVID-19, did not find a clinical benefit of CCP but found that antibody-dependent cell cytotoxicity (ADCC) was associated with a lower risk of intubation or death by day 30.<sup>12</sup> This suggests that the efficacy of CCP may in part depend on antibody Fc-effector functions and needs to be further investigated.

Previous studies have highlighted the remarkable heterogeneity of SARS-CoV-2-specific antibody titers and antibody-effector functions.<sup>13</sup> However, whether particular functions or antibody qualities, including ADCC, are associated with differential



therapeutic outcomes remains incompletely understood. We applied system serology to an open-label randomized clinical trial that had shown evidence of a mortality benefit from treatment with receptor-binding domain (RBD) ELISA-selected CCP treatment.<sup>14</sup> We found that CCP treatment delayed the evolution of Spike (S)-specific inflammatory antibody responses and induced stronger nucleocapsid (N)-specific antibody responses. Both of these changes were associated with improved outcomes in CCP-treated patients. We found that participants with lower pre-existing antibody function rather than low antibody levels experienced the greatest clinical benefit from CCP. It is clear that CCP modulated humoral immunity during acute disease and months thereafter, leading to more anti-inflammatory S-specific Fc glycans and persistent N-specific immunodominance.

## RESULTS

### Global SARS-CoV-2 humoral profiles of CCP-treated and control participants

With the emergence of novel SARS-CoV-2 variants that can escape vaccine-induced neutralizing antibody responses and monoclonal antibody therapeutic agents, CCP has regained attention as a potential therapeutic strategy to treat COVID-19.<sup>15–17</sup> However, clinical trials evaluating the efficacy of CCP have had mixed results. The striking heterogeneity of CCP and our incomplete understanding of the mechanisms of action of this natural therapeutic agent are contributing factors.<sup>12,13,18–20</sup> To attain a more granular understanding of the CCP properties that contribute to therapeutic efficacy, we profiled the SARS-CoV-2-specific antibody response across a group of patients enrolled in a randomized control trial of CCP conducted at the University of Pennsylvania.<sup>14</sup> The University of Pennsylvania (UPenn) CCP2 trial enrolled 80 individuals hospitalized with COVID-19 pneumonia, which is defined as a positive SARS-CoV-2 PCR assay, saturation of oxygen (SaO<sub>2</sub>) of less than 93% on room air or supplemental oxygen use, and radiological evidence of pneumonia (Figure 1A). Seventy-nine participants were included in our final analysis, 40 of whom were randomized to receive two units of CCP plus standard of care treatment and 39 of whom received standard of care treatment alone. One patient declined CCP treatment and withdrew from the study early. Participants' median age was 63 years (interquartile range [IQR] [52, 74]), 54% were female, 13% were on immunomodulatory treatments at baseline, and 26% had a prior cancer diagnosis. Prior to CCP randomization, 81% of participants had been treated with remdesivir, and 83% of participants had been treated with corticosteroids.

The UPenn CCP2 trial enrolled participants early in their disease course, the median of which was 6 days after symptom onset and 1 day of hospitalization. Mortality and the clinical severity score (CSC) were the two prespecified outcomes of this trial.<sup>14</sup> The clinical severity score (CSC) is a composite score that aims to effectively rank patients based on their disease severity, taking into account multiple endpoints in a prioritized manner.<sup>21</sup> The CSC in this trial took into consideration a participant's survival time, recovery time, and disease course while in the hospital, including the 8-point World Health Organization

(WHO) ordinal score (WHO8), use of supplemental oxygen, and adverse events. The CSC was found to be significantly different between CCP recipients and control individuals (median [IQR] 7 [2.75, 12.5] vs. 10 [5.5, 30],  $p = 0.037$  by Wilcoxon rank-sum test) (Figure 1B).<sup>14</sup> The study also found a mortality benefit associated with CCP administration on day 28 (odds ratio [OR] 0.156,  $p = 0.013$ ), with 5% (2 of 40) vs. 25.6% (10 of 39) mortality in CCP-treated vs. control participants. These clinically meaningful outcomes provided an opportunity to comprehensively examine the immunological profiles across CCP-treated and control participants to define potential biomarkers of immunity.

We profiled SARS-CoV-2-specific responses across CCP-treated and control participants using systems serology.<sup>13,22</sup> Antigen-specific isotype (immunoglobulin M [IgM] and IgA), subclass (IgG1, IgG2, IgG3, and IgG4), and Fc receptor binding (Fc $\gamma$ R2AH, Fc $\gamma$ R2B, Fc $\gamma$ R3AV, Fc $\gamma$ R3B, Fc alpha receptor 1 [FcAR], and neonatal Fc receptor [FcRn]) analyses were performed against S, the S1 domain of S, the RBD of S, the N-terminal domain (NTD) of S, and N across plasma samples from CCP recipients and control patients. Samples were taken when patients were enrolled into the study (pre-CCP or day 1, mentioned later) and on day 3, day 8, day 15, day 29, and day 60 after enrollment (Figure 1A). Antibody-directed innate immune cell functional analysis was performed over time against S and N, including antibody-dependent complement deposition (ADCD), antibody-dependent cell phagocytosis (ADCP), antibody-dependent neutrophil phagocytosis (ADNP), and antibody-dependent natural killer (NK) (ADNK) cell activation (Figure 1C).

As expected, the humoral immune response to SARS-CoV-2 evolved across all participants (Figures 1C and 1D). Nearly all S- and N-specific antibody features increased in the first 2 weeks of SARS-CoV-2 infection (Figure 1C). Multivariate uniform manifold approximation and projection (UMAP) visualization highlighted the similarities of the two profiled groups at the start of the study, with most day 1 samples (red) at the top in Figure 1D and most day 60 samples (green) at the bottom. These data support our assertion that timing of COVID-19 illness resulted in significant changes in humoral immune responses over time in this cohort. Samples from the CCP-treated and control arms of the study were intermixed throughout the UMAP visualization (Figure 1E), necessitating a more detailed analysis to identify whether the evolution of the SARS-CoV-2 specific humoral immune response differed between CCP-treated and control participants.

### CCP results in a delay in development of SARS-CoV-2 anti-S inflammatory antibody profiles

First, we confirmed that CCP-treated and control participants had similar pre-existing (day 1) anti-SARS-CoV-2-specific antibody profiles using UMAP plots (Figure 2A), local inverse Simpson's index (LISI) score analysis (Figure S1A), and univariate statistical testing (Figure S1B). Next, we focused on the early evolutionary differences across the groups, over the first 2 weeks of the trial, to understand how the trajectories of the humoral immune response differed across the two groups. When we looked at the distribution of how long patients had symptomatic COVID-19 prior to enrollment, we found that it varied greatly from 1–20 days (Figure S1C). Thus, we aligned all participant humoral

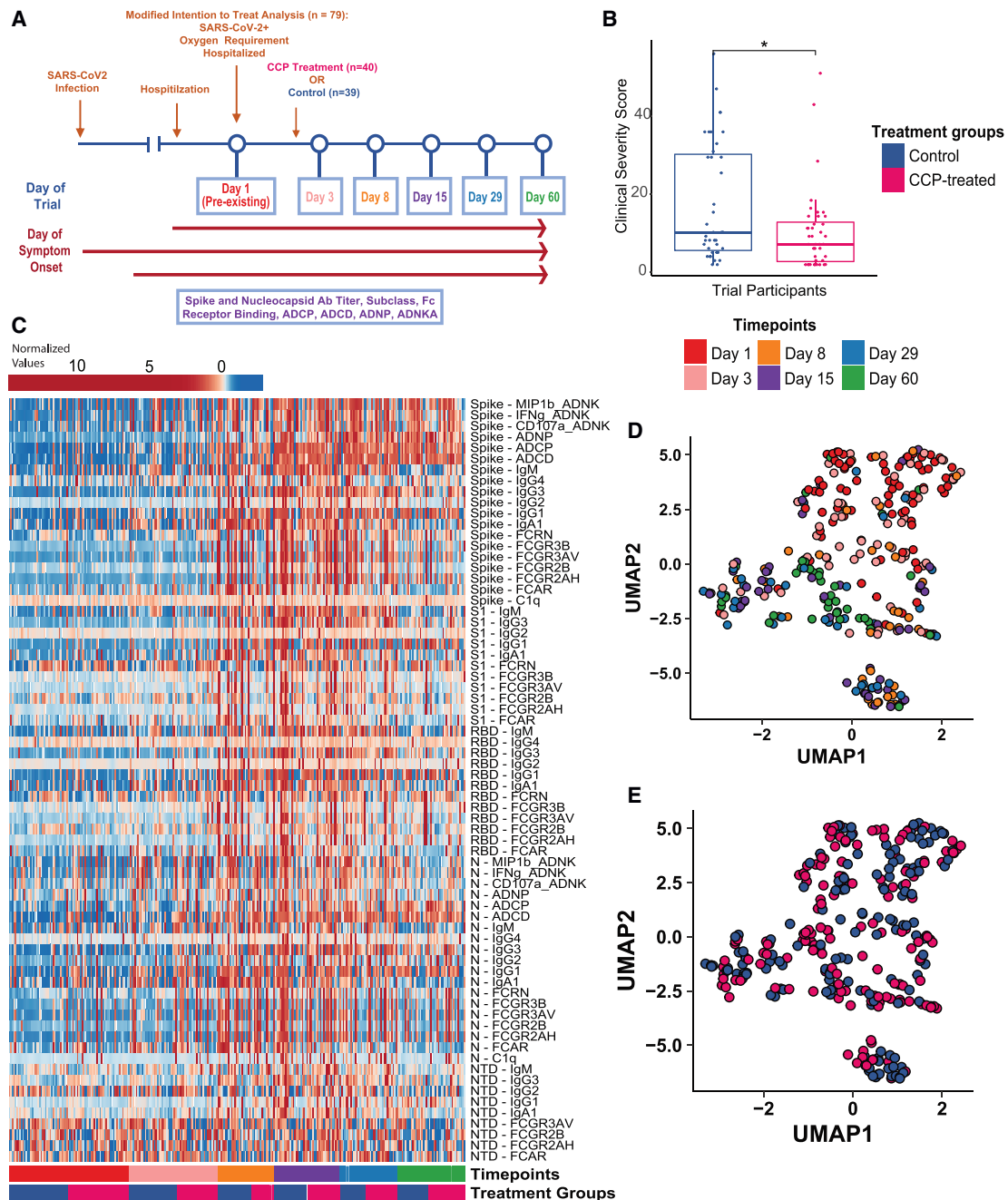


**Figure 1. Global anti-SARS-CoV2 response in CCP-treated and control individuals**

(A) Schematic of the UPenn CCP2 randomized clinical trial of CCP and the Ab profiling performed in this paper. In total, we profiled 302 samples from 79 patients. Patients were randomly assigned to CP treatment (n = 40) or standard of care treatment (n = 39). Patient serum samples were collected on day 1 (n = 79), day 3 (n = 59), day 8 (n = 37), day 15 (n = 44), day 29 (n = 38), and day 60 (n = 45). Because patients experienced symptomatic COVID-19 for a variable number of days prior to presenting to the hospital, we organized patient serum samples by day of the trial (day = 1 enrollment in clinical trial) and by day of symptom onset (day 1 = first day of COVID-19-associated symptoms).

(B) Clinical severity score in the CCP-treated and control groups. Significance corresponds to two-sided Wilcoxon test p values (p = 0.0333; \*p < 0.05).

(C) Heatmap of the SARS-CoV-2-specific Ab profiles of all patient time points, arranged by time point, arm of the trial, and patient age. Each bar represents the average of Ab measurements taken in technical duplicates (Ab level and FcR binding assays) and biological duplicate (ADCP, ADNP, and ADNKA).

(D and E) Uniform manifold approximation and projection (UMAP) was used to visualize the multivariate SARS-CoV-2 Ab profiles in two dimensions. Each point represents a given patient time point, and colors indicate (D) time point of collection and (E) treatment group.

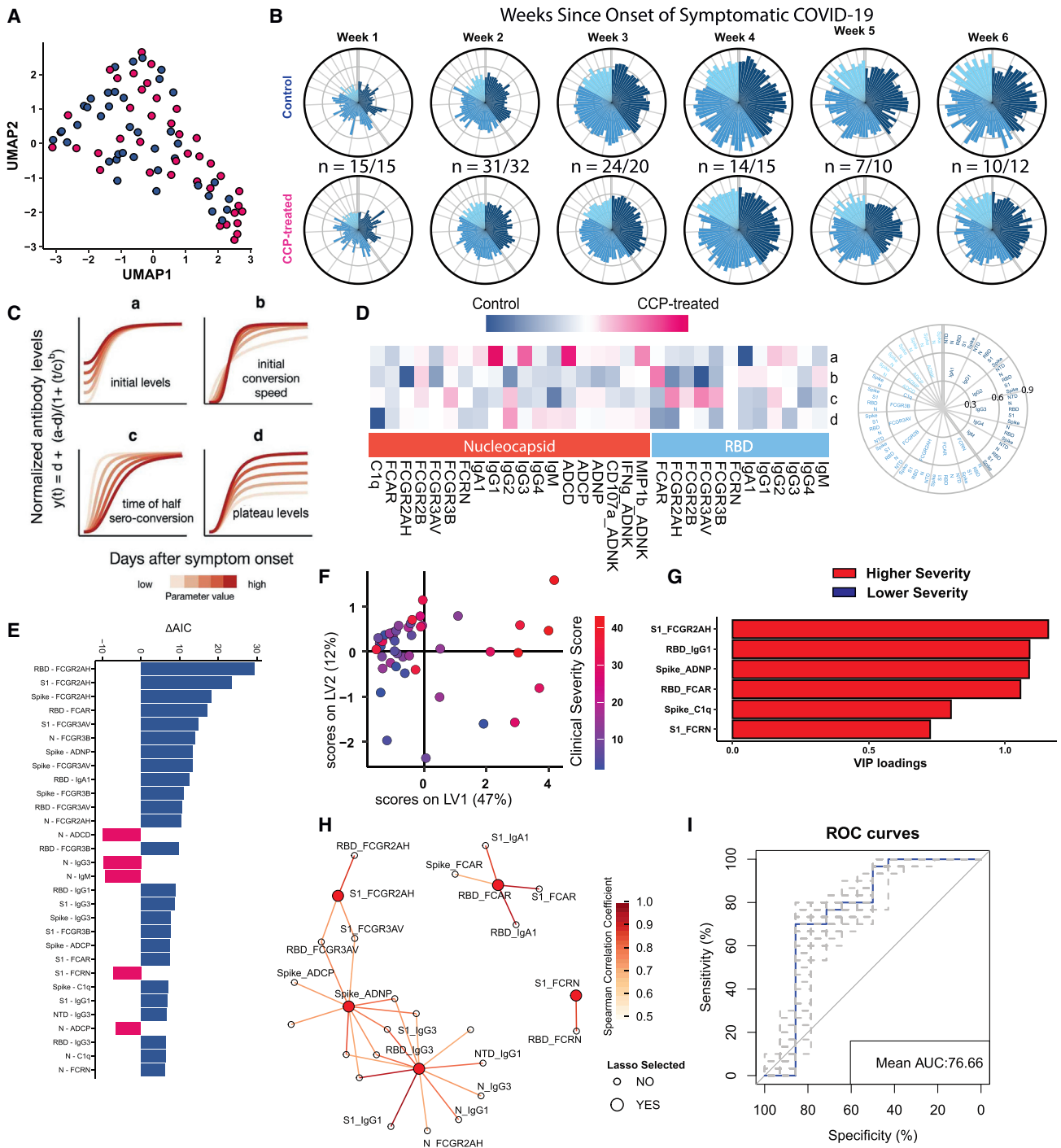


**Figure 2. CCP provides clinical benefits by limiting development of the inflammatory S Ab trajectory**

(A) Investigation of pre-existing (day 1) S Ab profiles by UMAP visualization of the samples on day 1 (pre-existing).

(B) The polar plots depict the mean percentile of each Ab feature at each week since onset of symptoms across the control arm (top) and CCP treatment arm (bottom). Numbers of patient samples included per time point are as follows (week [# control, # CCP treated]): week 1 (15, 15), week 2 (31, 32), week 3 (24, 20), week 4 (14, 15), week 5 (7, 10), and week 6 (10, 12).

(C–E) We employed a four-parameter logistic regression to fit the Ab growth trajectories to dissect the time-specific differences between CCP-treated and control patients for each Ab feature. (C) A visual representation of the logistic regression model and the effect of each parameter on the curve of the model.

(D) This heatmap shows the Akaike weighted average parameter differences between the two groups. Each column shows a parameter, which is normalized across the features. The color intensity indicates whether the parameter is higher in the CCP-treated (blue) or control (orange) model.

(legend continued on next page)

profile data by the time from onset of symptoms prior to randomization to adjust for heterogeneity in each participant's time from COVID-19 symptom onset. Using this approach we found that, by week 3 after symptom onset, CCP-treated individuals had lower S-specific titers, FcR binding, and antibody (Ab)-dependent functional activity (Figure 2B). This delay in the evolution of the S-specific response was also evident on day 8, when data were analyzed agnostic of day of symptom onset (Figure S1C).

To gain more granular insight into the specific humoral immune responses that evolved differentially across the two groups, four-parameter logistic regression models were generated for each Ab feature across each group from week 1 to week 4 from symptom onset.<sup>23</sup> This modeling approach allowed us to quantitatively define how CCP treatment led to differences in (1) initial levels of Ab features, (2) the initial speed of developing an Ab feature, (3) the time it took for seroconversion, or (4) final Ab feature plateau levels (Figure 2C). Although initial quantities and initial conversion speeds were mixed for RBD and N features, final RBD-specific titers (4, plateau level) and FcR binding (Fc $\gamma$ R2a, Fc $\alpha$ R, and Fc $\gamma$ R3b) were largely higher in the control population (Figures 2D, S1F, and S2). In contrast, N-specific titers and Ab plateau levels were similar in the two groups or slightly higher in CCP-treated individuals. Specifically, N-specific IgM, IgG2, and Fc $\gamma$ R3b binding levels were elevated in CCP-treated participants (Figures 2D and S1F). These data suggested that CCP treatment was associated with blunting of the inflammatory anti-S-specific humoral immune profiles in a manner distinct from N-specific humoral immunity.

To stratify individual humoral characteristics that differed most across the CCP-treated and control groups over time, we used the Akaike information criterion (AIC) of the paired models (Figures 2E and S2E). We found that S-, RBD-, and S1-specific Fc $\gamma$ R2a binding differed most between the two treatment arms (Figures 2E and S2). CCP-treated individuals exhibited lower levels and delayed evolution of S-specific Fc $\gamma$ R2a binding Abs (Figures 2E and S2). Conversely, N-specific ADCD, IgG3, and IgM differed between the two models and were enhanced in CCP-treated individuals (Figures 2E and S2). Specifically, N-specific IgG3 and N-specific ADCD developed earlier in CCP-treated individuals, and N-specific ADCD reached higher levels in CCP-treated individuals (Figure S2). By using a population-based logistic regression model, we found strong evidence

that CCP treatment resulted in attenuated inflammatory anti-S immune evolution. Dampened anti-S profiles were also linked to selectively enhanced N-specific humoral immune features.

### CCP-induced blunting of S-specific inflammatory Ab features is associated with improved clinical outcomes

Given the differences observed in S- and N-specific humoral immune evolution between the CCP-treated and control groups, we then sought to understand whether Ab properties enriched and depleted in CCP-treated participants were associated with improved clinical outcomes (measured by CSC) in CCP-treated and control participants.<sup>14</sup> Specifically, we selected the 30 Ab features with the greatest  $|\Delta\text{AIC}|$  values (Figure 2E). A least absolute shrinkage and selection operator (LASSO) was then applied to identify the minimal features that differed most across the CSC score at week 3 after symptom onset, and a partial least-squares regression (PLS-R) was applied to evaluate the association between CSC and the set of LASSO-selected features (Figure 2F). The PLS-R model identified differences between the groups that were statistically significant (Figures S1F and S1G). Only six of the top 30 AIC-selected features were sufficient to separate all participants based on CSC scores, including S1-specific Fc $\gamma$ R2a binding Ab levels, RBD-specific IgG1 levels, S-specific ADNP, RBD-specific Fc $\alpha$ R binding levels, S-specific C1q binding levels, and S1-specific FcRn binding. These six features were enriched in controls (Figure 2G) and in those with the most severe disease, defined as participants with a CSC of less than 20 (Figure 2I).

To identify the particular Ab properties associated with treatment benefits, we then investigated the associations of the minimal LASSO-selected Ab features with other Ab qualities within the larger humoral immune response using co-correlation networks. A large co-correlation network connected three of the LASSO-selected features: S1-specific Fc $\gamma$ R2AH, S ADNP, and RBD IgG1 (Figure 2H). This co-correlation network contained a broad and highly inflammatory S/RBD/S1-specific humoral profile, including more functional Ab subclasses (IgG1 and IgG3), S-specific neutrophil activity (ADNP), and S-specific monocyte responses (FcR2A and ADCP). A second tight co-correlation network linked RBD-specific Fc $\alpha$ R binding levels with S-, S1-, and RBD-specific IgA/Fc $\alpha$ R features, confirming prior observations that RBD/S-specific IgA responses are associated with

(E) The bar plot depicts the delta-AIC of the best model compared with the model without differences. The higher the delta-AIC, the better the model can explain the trajectory difference. The sign of delta-AIC represents the AUC difference between the CCP-treated and control curves, showing whether the Ab feature is enriched in the CCP-treated model (negative) or the control model (positive). The bars are colored according to whether the feature was enriched in the CCP-treated model (pink) or control model (blue).

(F–I) Partial Least Squares regression [PLS-R] model that predicts clinical severity in CCP-treated and control patients based on the top 30 features suggested by the four-parameter logistic model. The PLS-R model uses SARS-CoV-2 humoral profiles from week 3 since onset of symptomatic COVID-19. (F) The score plot of PLS-R regression shows the separation of week 3 samples along the continuum of clinical severity. Each dot represents a patient. (G) The bar graph shows the variable importance in projection (VIP) score in the PLS-R model of the LASSO-selected features. Features are colored by disease severity: features enriched in patients with higher severity (CSC > 20, red) or lower severity (CSC  $\leq$  20, blue) of COVID-19. (H) The network diagram illustrates the co-correlated features that are significantly correlated with the LASSO-selected features (larger nodes) ( $p < 0.05$  after multiple test correction using the Benjamini-Hochberg procedure, Spearman correlation coefficient > 0.7). Nodes enriched in patients with higher severity or lower severity of COVID-19 are colored red and blue, respectively. (I) The receiver operating characteristic [ROC] curve represents the predictive ability of the LASSO-selected S features (S1 FcR2AH, RBD IgG1, S ADNP, RBD FcR, S C1q, and S1 FcRn) to distinguish a higher severity score (CSC > 20) from a low severity score (CSC  $\leq$  20) using the PLS-DA model. Five-fold cross-validations were run 100 times, achieving a mean area under the curve (AUC) of 76.6. The blue line represents the mean ROC curve, and the dotted lines represent individual cross-validation ROC curves. All Ab measurements were taken in technical duplicates (Ab level and FcR binding assays) and biological duplicates (ADCP, ADNP, and ADNKA) and used as an average of the two for the analysis in this figure.

worse disease severity.<sup>24–27</sup> A third network consisted of RBD- and S1-specific binding to the FcRn. These three co-correlation networks consistently highlight the expanded and highly inflammatory S-specific humoral immune responses in individuals with the most severe COVID-19 (highest CSC).

We next investigated whether features associated with poor clinical outcomes in non-CCP-treated individuals were generalizable. To this end, we tested whether a PLS-R model based only on CCP recipients could predict poor clinical outcomes for all trial participants. Specifically, we used the above PLS-R to predict whether participants, regardless of CCP treatment, could be classified into (1) high-severity COVID-19 outcome (CSC > 20) or (2) low-severity COVID-19 (CSC ≤ 20). The model was highly predictive of disease severity, achieving an average area under the curve (AUC) in a receiver operating characteristic [ROC] curve of 77% (Figure 2I). This demonstrated that these six inflammatory S Ab features predicted worse COVID-19 clinical outcomes and reinforces that the inflammatory S Ab features in control participants are associated with more severe outcomes. Thus, CCP modulation of S humoral immunity and dampening of inflammation are linked to improved disease outcomes.

#### Correction for co-morbidities points to a robust N-specific Ab signature of CCP treatment

A major challenge in understanding the effect of CCP is the heterogeneity of COVID-19 clinical disease. Co-morbid conditions, including obesity, diabetes, cardiovascular disease, chronic kidney disease, concomitant immunosuppression, and cancer, have been associated with more severe COVID-19.<sup>28</sup> Age and obesity have been associated with decreased B cell responses and lower Ab responses to pathogens and vaccines.<sup>29</sup> To account for these covariates in our analysis of CCP-induced humoral immune evolution, we used a nested mixed-linear modeling approach of the Ab profiles of CCP-treated and control participants over the first 15 days of the study (days 1–15 of the clinical trial). Age, sex, race, ethnicity (Latinx vs. non-Latinx), blood type, quarter of enrollment, diabetes, cardiovascular disease, hypertension, obesity, chronic kidney disease, cancer, prior immunosuppression, concomitant treatment with remdesivir at study entry, concomitant treatment with steroids at study entry, and time of symptom onset were included in the models. For each Ab feature, we generated two mixed linear models. The full model incorporated treatment group (CCP treatment vs. control) as a fixed effect; the null model, on the other hand, did not. Then we compared the two nested models with the likelihood ratio test (LRT) to identify Ab features whose trajectories were affected by CCP treatment. We then extracted the T values (normalized coefficient) of the treatment group variable in the full mixed linear model to quantify the CCP treatment effect on Ab features. Ab features significantly affected by CCP treatment were defined as having a T value greater than 2 and a two-sided p value of less than 0.05. Most Ab features that significantly differed between CCP-treated and control individuals were enriched in CCP-treated individuals (Figure 3A), suggesting that many of the S-specific features that increased in control individuals (Figure 2F) were influenced by known COVID-19 disease severity risk factors. Most features enriched in CCP-treated individuals were N-specific Ab features, including binding strength

to N-specific-FcγR2B, -FcγR3B, and -ADCC. The only feature enriched in control participants (T < -2) was RBD Ab binding to the IgA FcR FcαR (Figure 3A), also identified in our modeling based on days from symptom onset (Figure 2F). To ensure the validity of the model results, we next confirmed that the N feature levels prior to randomization were balanced across the two arms (Figures 3B and S3A). Thus, using a multivariate mixed-effects model, a robust and unexpected N-specific humoral signature emerged in CCP-treated participants.

#### N features are associated with improved outcomes in CCP-treated and control participants

Given the enrichment of N-specific Ab features in CCP recipients, we next sought to understand the relationship between N-specific Abs and clinical outcomes in all study participants. To define whether certain N-specific Ab features were associated with specific clinical outcomes, we applied a linear effects model to the N-specific Ab profiles of CCP-recipients and controls over the first 2 weeks of the trial (days 1–15). Data were corrected for co-morbidities associated with COVID-19. N-specific features explained 30% of the variation in clinical outcome across the cohort (Figure 3C). The association of individual N-specific Ab features and clinical outcome (CSC) (Figure 3D) pointed to an association between most N-specific Ab features and better clinical outcomes. Specifically, N-specific ADCC, the most strongly CCP-enriched Ab feature (Figure 3A), was also one of the most strongly associated with better clinical outcomes (Figure 3D). N-specific FcγR2B, FcγR3B, C1q binding, and IgM titers were also enriched in CCP-treated individuals and associated with improved clinical outcomes (Figures 3A and 3D). On the other hand, N-specific NK cell CD107a and MIP1b expression were most strongly associated with better outcomes (Figure 3D) but not differentially enriched between CCP-treated and control participants (Figures 2F and 3A), suggesting that N-specific ADCC may be beneficial in COVID-19 but not affected by CCP treatment. Not all N-specific Ab responses are beneficial. N-specific IgA and IgG4 levels were not enriched in CCP-treated individuals and were associated with worse outcomes. These analyses suggest that particular CCP treatment-associated N-specific humoral immune responses are associated with better clinical outcomes.

#### COVID-19 participants with low functional Abs benefitted most from CCP treatment

Emerging data from clinical trials suggest that participants who have not yet generated an Ab response to SARS-CoV2 may benefit the most from monoclonal Ab therapy.<sup>3,10,30,31</sup> We sought to understand whether seronegative individuals also benefitted from CCP treatment. Next, to understand which participants benefitted the most from CCP therapy in this study, participants were clustered based on their day 1 SARS-CoV-2 Ab profiles. We used a Spearman correlation distance-based neighborhood clustering approach (Figure 4A). Four clusters of participants with similar pre-existing Ab profiles appeared (Figures S4A and S4B). Cluster 1 contained participants with the highest S- and N-specific humoral responses, and clusters 2, 3, and 4 had more varied Ab profiles. Cluster 4 included individuals with the lowest S and N titers across all Ab features

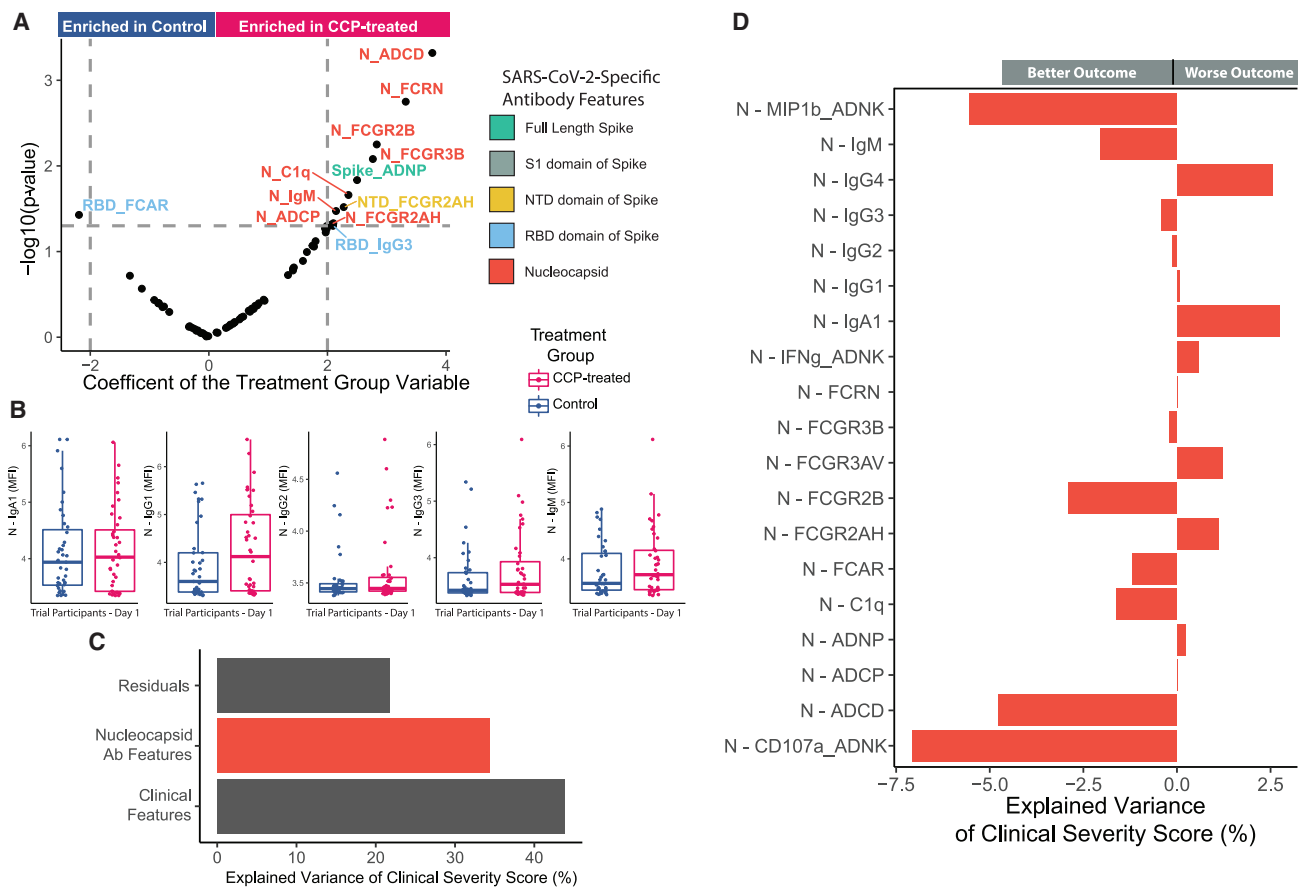


**Figure 3. CCP also provides clinical benefits by enhancing N-focused humoral response**

A nested mixed linear model was created for each Ab feature with and without a variable accounting for patient’s treatment group (CCP treatment versus control) to assess CCP effects on host anti-SARS-CoV-2 humoral development.

(A) Volcano plot showing the T value (normalized coefficient) of the patient treatment group variable incorporated in the mixed linear model (x axis) and p value of the LRT for the model fit difference between the two nested models (y axis). A positive T value represents a feature enriched in CCP-treated individuals, and a negative T-value represents a feature enriched in control individuals.

(B–D) (B and C) N-specific humoral profile of CCP-treated and control patients. (B) Boxplots of selected N-specific features prior to treatment (day 1). Each box represents the median (central line) and IQR (25th and 75th percentiles), and the two whiskers represent  $1.5 \times$  IQR. (C and D) A Linear regression model was used to assess whether N features could predict COVID-19 clinical severity of CCP-treated and control patients as measured by the clinical severity score. (C) The bar plot shows the percentage of explained variance by clinical data (clinical characteristics, severity risk factors, and concurrent medications) and N Ab features. (D) The bar plot shows the contribution of each N Ab feature to COVID-19 clinical severity. The magnitude represents the percentage of variation in the clinical severity score explained by each feature, and the directions represents whether the Ab feature was associated with better (i.e., negative explained variance of clinical severity score [%]) or worse (i.e., positive explained variance of clinical severity score [%]) clinical outcomes. All Ab measurements were taken in technical duplicates (Ab level and FcR binding assays) and biological duplicates (ADCP, ADNP, and ADNKA) and used as an average of the two for the analysis in this figure.

(Figure 4A). Principal-component analysis and co-correlation network structure demonstrated that clusters 1 and 4 were most distinct in their SARS-CoV-2 Ab profiles (Figures 4B and S4B). CCP-treated participants in cluster 4 exhibited the greatest benefits (lower CSC) compared with control participants (Figures 4C and 4F). To gain a granular sense of how cluster 4 individuals differed from the other clusters, we performed univariate testing comparing cluster 4 Ab profiles with the Ab profiles of non-cluster 4 participants, including clusters 1, 2, and 3 (Figures 4D, 4E, and S5). Specifically, cluster 4 participants possessed lower S- and N-specific Ab functions. They also exhibited the lowest S- and N-specific ADCP, low S- and N-specific Ab-mediated NK cell MIP1b production, and lower

S- and N-specific IgA1 and IgG1 titers (Figures 4D, 4E, and S5). Based on these observations, we created the CCP benefit signature: the set of features that best distinguished cluster 4 from clusters 1, 2, and 3. The CCP benefit signature included all N- and S-specific Ab functional measurements and all Ab titers with  $|\log \text{fold change [FC]}| > 0.75$  (N-IgG1 and N-IgA1). Our results suggested that participants with lower functional Ab responses were more likely to benefit from CCP treatment.

Additional comparisons of clinical factors across the four clusters pointed to a relatively balanced symptom duration prior to trial enrollment (Figure S4C). However, participants in cluster 4 were less likely to have chronic kidney disease (CKD), be obese, or be African American. On the other hand, they were more likely

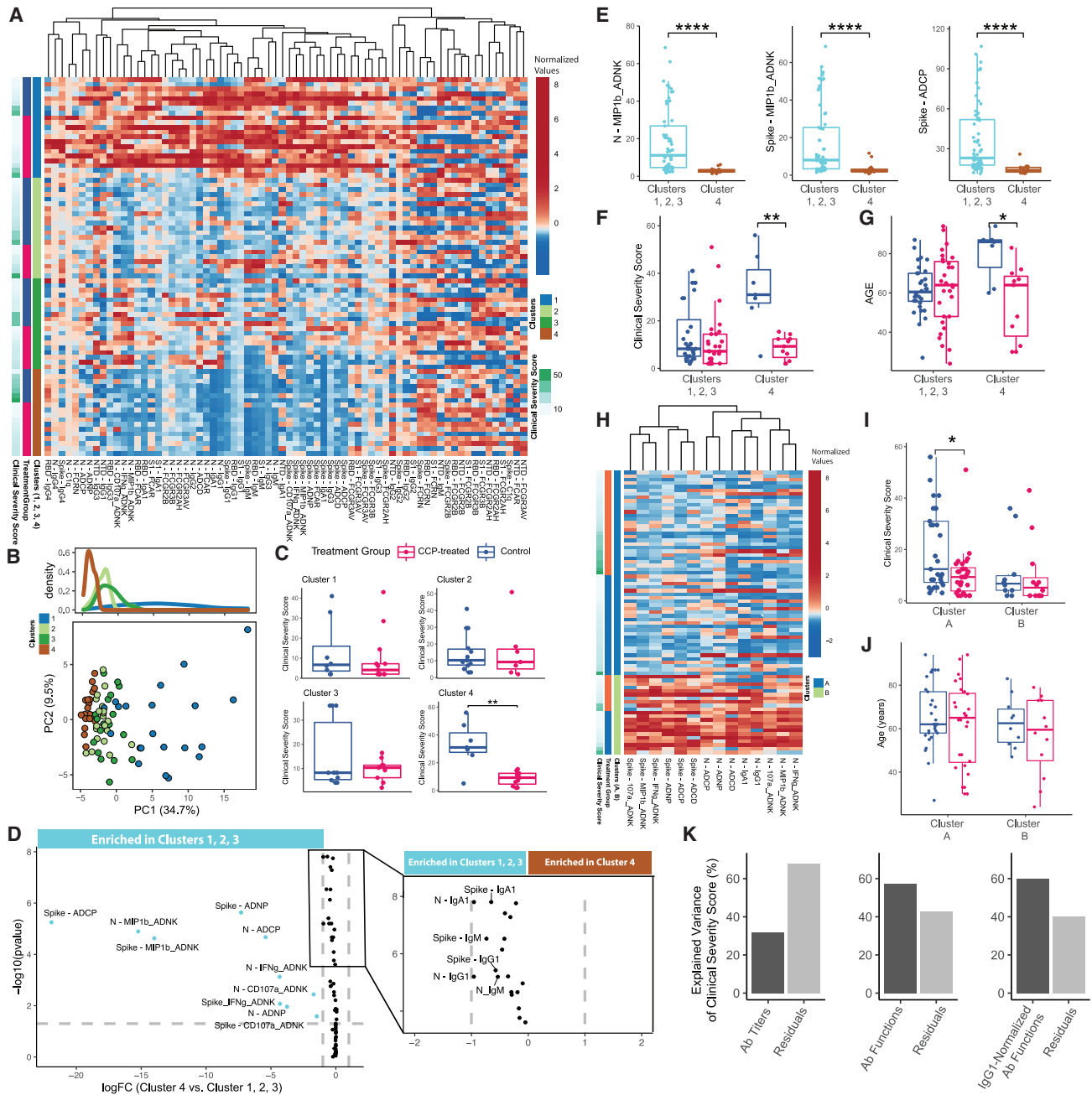


**Figure 4. Patients with fewer functional pre-existing Abs benefit the most from CCP**

(A–F) Seventy-nine samples collected before treatment (day 1) were used to evaluate the association between Ab profiles and clinical severity, as measured by the clinical severity score on day 28. Spearman correlation-based clustering was used to identify the population benefitting from CCP. (A) The heatmap represents the normalized day 1 Ab profiles. Patient samples were clustered into four groups based on the similarity of Spearman correlation coefficients of day 1 SARS-CoV-2 Ab profiles between samples.

(B) Principal-component analysis (PCA) plot (bottom) shows the relatedness of patients in each of the identified four clusters, and the density plot (top) displays the organization of the patient samples from each of the four clusters along principal component 1 (PC1). (C) The boxplots show the clinical severity scores of CCP-treated and control patients in each of the four clusters. A Wilcoxon rank test was used to test for differences in clinical severity scores between the two groups in each cluster (two-sided p value: 0.365, 0.799, 1, 0.00415). (D) The volcano plots show the Ab function, titers, and FcR binding features that were most different between cluster 4 and the rest of the population (clusters 1, 2, and 3). The pop-out highlights features with a log fold change (logFC) between  $-2$  and  $2$  as well as  $p < 0.05$ . The x axis represents the logFC of cluster 4 over clusters 1, 2, and 3, and the y axis represents the p value from a two-sided Wilcoxon test. Each dot represents an Ab feature. Ab features with  $|\logFC| > 2$  are colored according to the population in which they were enriched; i.e., in cluster 4 (brown) or in

(legend continued on next page)

to have enrolled later in the clinical trial period (May 2020 through January 2021) (Table S1). Cluster 4 control individuals were significantly older than the individuals in the cluster 4 CCP-treated group (Figure 4G; Table S2). To define whether the CCP response signatures identified in cluster 4 could predict benefits from CCP across the whole trial, we re-clustered participants based on the CCP benefit signature. Ab profiles clustered into 2 groups (Figures 4H, S4D, and S4E). Cluster A consisted of a heterogeneous mix of participants with overall lower S- and N-specific Ab features (Figure 4H) and with statistically significant lower CSC (and better clinical outcome) in CCP-treated participants (Figure 4F). In contrast, cluster B consisted predominantly of higher levels of S- and N-specific Ab functions and titers (Figure 4H) and nearly identical CSC across CCP-treated and control participants (Figure 4I). Clinical characteristics were equally distributed across the two-cluster model (Table S3) as well as across cluster A CCP-treated and control groups (Table S4). These data suggest that the quality of the pre-existing humoral immune response to SARS-CoV-2 infection largely explained the benefit individuals received from CCP, rather than patient demographic factors or COVID-19 severity risk factors.

We next sought to identify specific pre-existing Ab functions or levels that were predictive of benefits from CCP treatment. We created three linear models that predicted the clinical severity measured by the CSC of CCP-treated participants based on their pre-existing Ab levels, unadjusted Ab functions, or IgG1-normalized Ab functions. For this comparison, we used the top 12 Ab functions and the top 12 Ab levels that differed between cluster 4 and clusters 1, 2, and 3 (Figure 4D). Ab isotype and subclass alone only predicted 32% of the variation in CSC, whereas Ab functions predicted 57% of variation in CSC (Figure 4K). When we normalized the Ab functions by IgG1 to eliminate the influence of Ab titer differences, we continued to explain 60% of the variation in CSC (Figure 4F). Although S IgG1 level was predictive (Figure S4), IgG1-normalized S- and N-specific humoral features, such as N-ADCP, N-ADNP, and S- as well as N-ADNKA MIP-1 $\beta$ , were more predictive (Figures S4G and S4H). This suggests that the magnitude of the pre-existing Ab functional humoral response was more predictive than sero-status alone.

SARS-CoV-2-specific Ab titers are tightly associated with disease severity.<sup>32–34</sup> Thus, to understand whether individuals with lower Ab levels represented a surrogate of lower viral

burden and, thus, a higher likelihood of surviving disease, we compared SARS-CoV-2 viral loads across cluster A and cluster B prior to CCP treatment. We found that, prior to CCP treatment, cluster B CCP recipients had lower nasopharyngeal swab viral loads than their cluster A counterparts (Figure S6A). SARS-CoV-2 viral loads were significantly anti-correlated with many S protein Ab titers but not with many S and N Ab functions (Figure S6B). We next found that Ab function and titer were far better predictors of clinical severity than SARS-CoV-2 viral load in a linear regression model, accounting for 41.5%, 15%, and 5.3% of the variation in clinical severity score, respectively (Figures S6C and S6D). Further, Ab functional measurements were better predictors of clinical severity than SARS-CoV-2 viral load. A single functional Ab measurement, N-ADNP, was 3-fold more predictive of clinical severity than SARS-CoV-2 viral load. Though higher viral loads have previously been shown to be predictors of clinical response to CCP therapy in prior work, here we found that pre-existing anti-SARS-CoV-2 functional humoral responses are stronger predictors of response to CCP.

### Two months later, CCP treatment resulted in a sustained shift in the inflammatory status of S-specific Ab via glycosylation changes

Based on the pharmacokinetics of intravenous immunoglobulin [IVIg] in secondary immunodeficiencies, it is unlikely that Ab from 2 units of CCP (~400 mL) would continue to circulate for more than a month after therapy.<sup>35</sup> Thus, we next examined whether CCP had long-lasting effects on recipients' SARS-CoV-2 humoral immune response. First we found that CCP-treated and control participants did not have significantly different S IgG1 levels (Figure 5A). In addition to changes in the overall levels of Abs, the functional and inflammatory properties of Abs are regulated by changes in IgG Fc glycosylation at asparagine 297.<sup>36–38</sup> Given the importance of the Fc glycan in severe COVID-19,<sup>39,40</sup> we profiled Fc glycan differences across CCP-treated and control participants 2 months after treatment (day 60). CCP-treated individuals exhibited selective enrichment of S-specific disialylated and diglycosylated peaks, such as G2S2F, G2S2B, and G2S21F (Figures 5B and 5C). A LASSO/PLS-DA model, using S-specific Fc glycan profile features only, was able to separate CCP-treated from control participants (Figures 5D and S7A). Among the Fc glycan structures, digalactosylated and sialylated structures were selectively enriched in CCP-treated participants, whereas asialylated G1FB.G2 was

clusters 1, 2, and 3 (cyan). (E) Boxplots of representative Ab functions enriched in non-cluster 4 patients. (F) Boxplot of the clinical severity score of CCP-treated and control patients in cluster 4 and clusters 1, 2, and 3. A two-sided Wilcoxon test was performed to compare age between treatment arms.

(G) Boxplot of the age of CCP-treated and control patient in cluster 4 and clusters 1, 2, and 3. A two-sided Wilcoxon test was performed to compare age between treatment arms.

(H–J) Re-clustering patients based on the benefit signature identified in (D) and (E) on the whole population. (H) The heatmap shows the two clusters (clusters A and B) identified by the benefit signature—the features that most distinguished cluster 4 from clusters 1, 2, and 3 patients (the top 12 features). (I) Boxplots of clinical severity of CCP-treated and control groups in clusters A and B. The difference between CCP-treated and control patients' clinical severity was tested by two-sided Wilcoxon test. (J) Boxplots of the age of CCP-treated and control groups in clusters A and B.

(K) Three separate linear regression models were used to assess which type of pre-existing Ab features best predicted clinical severity in CCP-treated individuals. The bar plots show the percentage of explained variance by Ab titers, Ab functions, or IgG1 titer-corrected Ab functions in the separate models. We used the top 12 features that differed between cluster 4 and clusters 1, 2, and 3 for the linear regression model of each Ab feature category.

For the boxplots in (C), (E)–(G), (I), and (J), each box represents the median (central line) and IQR (25th and 75th percentiles), and the two whiskers represent 1.5  $\times$  IQR. \* $p < 0.05$ , \*\* $p < 0.01$ , \*\*\* $p < 0.001$ , \*\*\*\* $p < 0.0001$ . All Ab measurements were taken in technical duplicates (Ab level and FcR binding assays) and biological duplicates (ADCP, ADNP, and ADNKA) and used as an average of the two for the analysis in this figure.

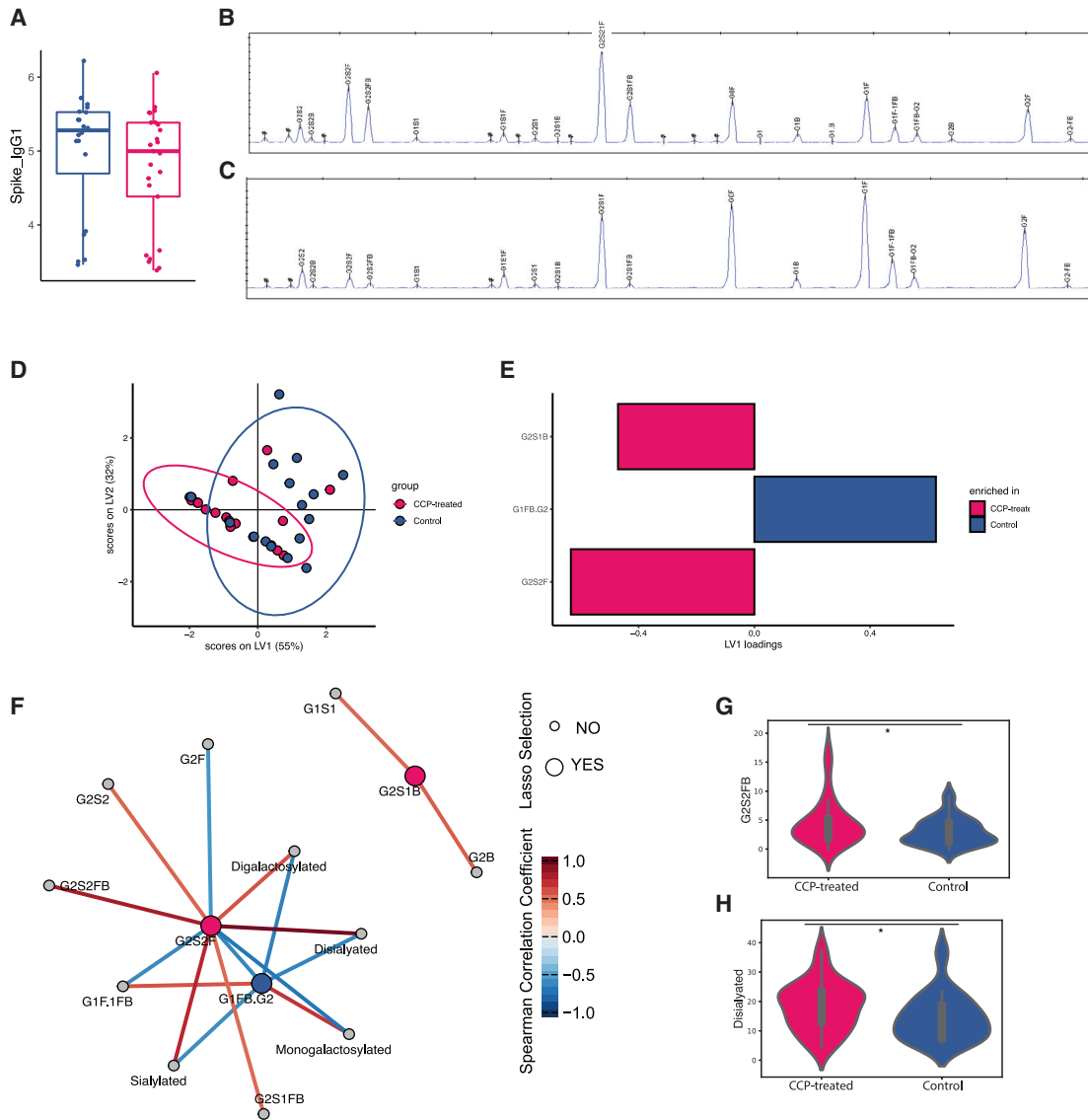


**Figure 5. CCP recipients have highly sialylated and galactosylated S-specific Fc modifications long after treatment**

(A–C) (A) Bar graphs of S-specific IgG1 levels in CCP-treated and control participants 60 days after randomization. S-specific Fc glycosylation patterns were measured by capillary electrophoresis in all participants with day 60 samples collected from CCP-treated ( $n = 19$ ) and control ( $n = 16$ ) participants. Shown are representative chromatographs of CCP-treated (B) and control (C) participants.

(D and E) LASSO PLS-DA was performed to identify the Fc glycan features that separated the two groups. The PLS-DA score plot (D) shows that the S-specific Fc glycans can separate CCP-treated from control participants, with LV1 explaining 41% of variation that separates the two groups along the x axis. Each dot shows an Fc glycan measurement. The LV1 loading plot (E) shows the LASSO-selected features. Pink represents features enriched in CCP-treated participants, and blue represents features enriched in control participants.

(F) The Spearman correlation network shows the co-correlated features (small nodes) that are significantly correlated ( $p < 0.05$  after multiple test correction using the Benjamini-Hochberg procedure, Spearman correlation coefficient  $> 0.5$ ) with the model-selected features (large nodes). Large nodes are colored according to the treatment arm in which they are enriched. Edges are colored by magnitude and sign of correlation, with dark red and dark blue representing strong correlation and anti-correlation, respectively.

(G and H) Univariate plots for G2S2FB (G) and disialylated (H) Fc glycans in CCP-treated (pink) and control (blue) participants.

\* $p < 0.05$  by a two-sided Wilcoxon rank test. All Fc glycan measurements are expressed as an average of technical duplicate capillary electrophoresis runs.

enriched in control participants (Figure 5E). A co-correlational network was constructed to gain deeper insights into the collection of Fc glycans that may co-evolve in the setting of CCP treatment (Figure 5F). G2S2F, enriched in CCP-treated par-

ticipants, was strongly correlated with sialylation, disialylation, digalactosylation, as well as individual digalactosylated Fc glycan species, including G2S1FB, G2S2, and G2S2FB. Conversely, G2S2F was strongly anti-correlated with monogalactosylation

and asialylated features such as G2F, G1F.1FB, and G1FB.G2, pointing to enrichment of heavily sialylated and galactosylated S Abs in CCP-treated individuals. Because high sialylation<sup>41,42</sup> and galactosylation<sup>43</sup> have been linked to anti-inflammatory Ab activity, these data point to the evolution of anti-inflammatory S-specific Ab profiles after CCP therapy. A second network was observed, including the CCP-treated enriched feature G2S1B with another bisected feature G2B, pointing to a potential role of bisecting GlcNAc in CCP-treated individuals. G2S2FB and disialylated Abs were individually significantly enriched in CCP-treated individuals compared with non-treated control individuals (Figures 5G and 5H). These data point to a longer-term effect of CCP on shaping the inflammatory profile of the evolving SARS-CoV-2 humoral immune response.

### N immunodominance persists 2 months after CCP treatment

Given the presence of a persistent anti-inflammatory humoral signature on S-specific Abs 2 months after treatment, we finally aimed to define whether early signatures of response to therapy persisted over time. Thus, we investigated the SARS-CoV-2-specific Ab profiles of CCP-treated and control participants 2 months after treatment. Two months after therapy, CCP-treated individuals continued to exhibit enhanced N-specific Ab titers and FcR binding Abs. Control participants still had higher S1- and RBD-specific Ab titers and FcR binding (Figures 6A and 6B), pointing to persistence of the immunodominant shift associated with CCP therapy. Using a LASSO/PLS-DA, we found that CCP-treated individuals continued to exhibit a unique overall humoral immune profile compared with control participants (Figures 6C–6E). Only 4 of the total 70 features were sufficient to separate Ab profiles across the 2 groups 2 months after therapy. Two features, NTD-specific IgA1 and NTD-specific Fc $\gamma$ R3A binding Ab levels, were enriched in control participants in our model (Figure 6D). N-specific IgM and C1q binding Abs were selectively enriched in CCP-treated individuals (Figure 6D). The LASSO-selected feature co-correlation network highlighted the presence of additional S-specific features associated with NTD-specific Fc $\gamma$ R3AV binding levels in control individuals. These features were inversely correlated with N-specific ADCP, highlighting the dichotomous response represented by an S- or N-focused Ab profile (Figure 6F). N-C1q was tightly co-correlated with 15 other N-specific Ab features that were all selectively enriched among CCP-treated individuals. The tight correlation of N-specific ADCD with C1q (Figure 6F), as well as the LASSO selection of N-specific C1q and N-specific IgM (Figure 6D), suggested that CCP treatment may contribute to a durable, classical complement pathway response. These data point to durable effects of CCP that result in long-lived attenuation of S-specific inflammatory responses in favor of a durable, N-specific, complement-focused humoral response. These data suggest that the benefits of CCP in hospitalized patients with COVID-19 are in part due to an immunodominance shift in humoral immune evolution. CCP treatment is marked by a reduced S-specific humoral immune response and augmented N-specific humoral immunity, resulting in durable changes in Ab profiles months after treatment.

### DISCUSSION

Since the start of the COVID-19 pandemic, many clinical trials have studied the efficacy of CCP. Many large studies of hospitalized patients with COVID-19 have not demonstrated benefits from CCP. However, select studies of high-titer CCP earlier in disease have shown a mortality benefit and improvement in clinical status.<sup>3–7,9–11,14</sup> We used systems serology to study a randomized study showing clinical benefits of CCP treatment early in hospitalization for COVID-19 pneumonia<sup>14</sup> to understand the signatures of protective immunity provided by CCP. Insight into the specific components of a polyclonal Ab therapy that are associated with improved patient outcomes could inform how we choose and design monoclonal Abs (mAbs) for future SARS-CoV-2 treatment therapies. We found that CCP shifted immunodominance to SARS-CoV-2 by diminishing the S-focused evolution in exchange for expanded N-specific activity. The clinical benefits associated with this immunodominance shift support three major findings: (1) the importance of blunting the inflammatory S-targeted humoral response in severe COVID-19 disease, (2) the critical role of N-specific immune complexes in CCP benefits, and (3) the anti-inflammatory effects on the S and N humoral response are long lasting. These findings expand our previous study earlier in the COVID-19 pandemic, which was not designed to assess the clinical benefits of CCP but found that CCP enriched in N-specific Abs blunted development of the inflammatory anti-SARS-CoV-2 host response.<sup>13</sup> Here, in the UPenn CCP2 study, we found that CCP treatment led to slower development and lower levels of FcR2A-binding Abs, the predominant FcR on monocytes, as well as lower levels of S-, S1-, and RBD-specific Abs, suggesting that CCP may actually blunt development of monocyte-activating S Abs. Emerging work has shown that the afucosylated inflammatory S Abs found in participants with severe COVID-19 promote macrophages to produce pro-inflammatory cytokines<sup>44</sup> and that inflammatory monocyte/macrophages are central to the hyperinflammatory state in severe COVID-19.<sup>45</sup> This strongly supports the possibility that part of the therapeutic benefit of a polyclonal Ab therapy occurs via immunomodulatory effects of the Abs rather than solely via antiviral activity alone. Thus, in some instances, CCP treatment therapy may acutely dampen the Ab-induced macrophage/monocyte hyperinflammatory host response, tempering the cytokine storm, and potentially result in long-lasting anti-inflammatory effects after resolution of COVID-19 viremia.

The underlying immunologic mechanisms of how CCP leads to long-lasting immunomodulation remain unclear but may include several non-mutually exclusive mechanisms. Blockade of viral spread by CCP-derived neutralizing Abs coupled to the opsonophagocytic activity of CCP-derived functional Abs may lead to attenuation of inflammation at the time of infection, permitting the immune system to develop a balanced adaptive immune response.<sup>46,47</sup> Now CCP is derived from convalescent individuals months from acute infection with rested, less inflammatory Fc domains. Conversely, it is plausible that CCP-formed immune complexes may also drive uptake via type 2 receptors,<sup>48–50</sup> germinal center activation, and clearance of the virus in the setting of anti-inflammatory signals that lead to epigenetic programs that result in longer-lived anti-inflammatory responses.<sup>51</sup> More work is

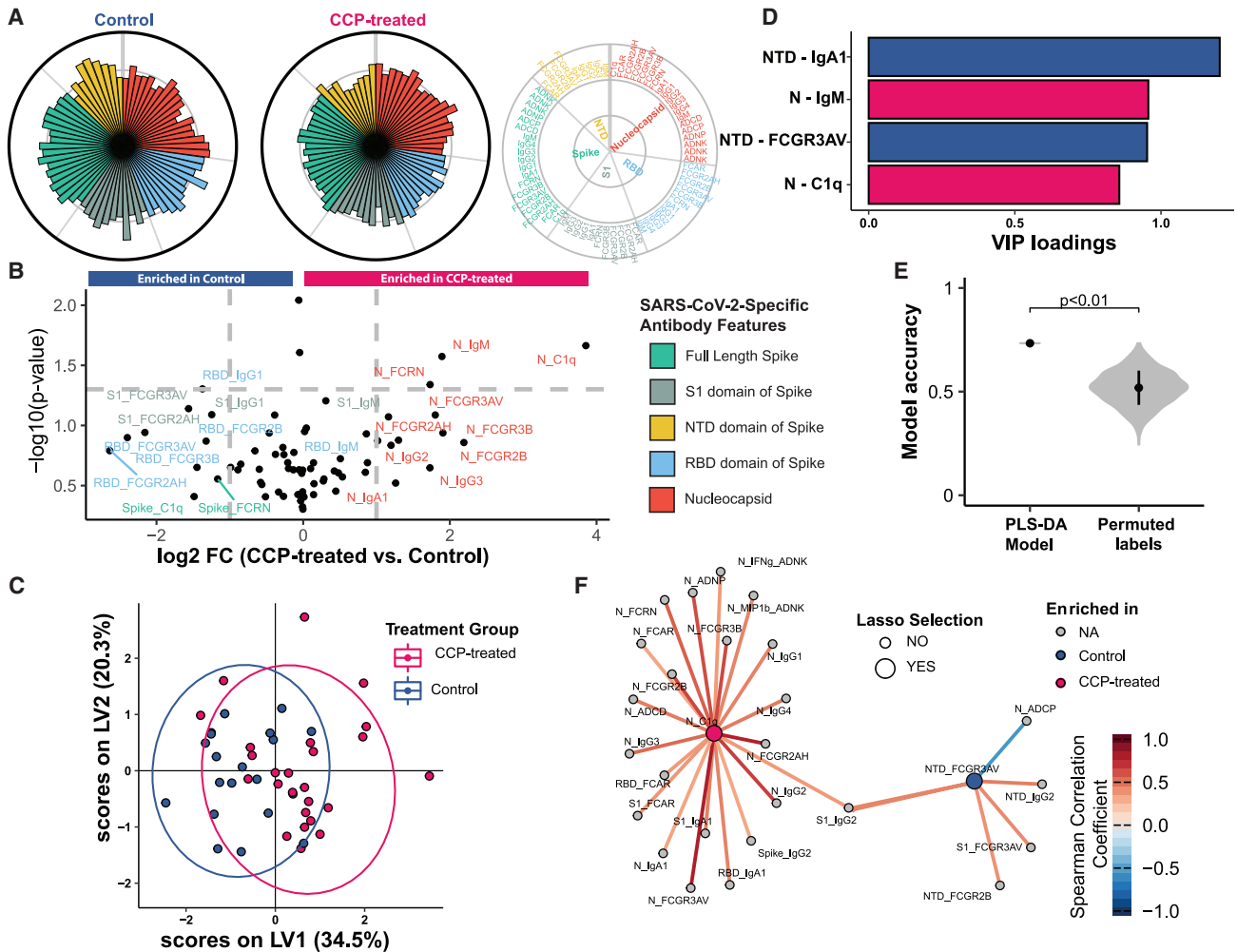


**Figure 6. Long-lasting N immunodominance in CCP recipients**

Shown are SARS-CoV-2 functional Ab profiles of 45 patients (CCP-treated, n = 25; control, n = 20) on day 60.

(A) Polar plots of the mean percentile of each Ab feature across the control (left) and CCP-treated study arms (right). The features were grouped by the antigen detectors and are depicted in a key.

(B) Volcano plot showing the difference between the humoral profile of the CCP-treated group and control group by the FC of mean value (x axis) and two-sided p value from Wilcoxon rank test (y axis).

(C–F) LASSO PLS-DA model identified the Ab features that distinguish CCP-treated from control patients on day 60. (C) The PLS-DA score plot demonstrates that CCP-treated and control day 60 patients can be discriminated by the LASSO-selected features. Each dot represents an individual patient. (D) VIP score of the selected features. The magnitude indicates the importance of the features in driving separation in the model. Pink represents a feature enriched in CCP-treated patients, and blue represents a feature enriched in control patients. (E) The performance and robustness of the model was validated with permutation testing. The violin plot shows the distributions of repeated classification accuracy testing using label permutation. The p value from the permutation testing is two sided. Black squares indicate the median accuracy and black lines represent 1 SD. (F) The correlation network shows the co-correlated features (small nodes) that are significantly correlated (p < 0.05 after multiple test correction using the Benjamini-Hochberg procedure, Spearman correlation coefficient > 0.3) with the model-selected features (large nodes). Large nodes are colored according to the treatment arm in which they are enriched. All Ab measurements were taken in technical duplicates (Ab level and FcR binding assays) and biologic duplicates (ADCP, ADNP, and ADNKA) and used as an average of the two for the analysis in this figure.

needed to elucidate the precise mechanism(s) by which CCP may regulate immunity beyond simple clearance of the virus. Our results show that N-focused immunodominance in COVID-19 disease is associated with improved clinical outcomes. Emerging work suggests that freely circulating N protein can activate complement via the alternative pathway<sup>52,53</sup> and is likely involved in the hyperinflammatory lung damage seen in people with severe COVID-19 that leads to acute respiratory

distress syndrome.<sup>52,54</sup> mAbs targeting N in an *in vitro* system can inhibit free N-induced MASP-2 activation.<sup>53</sup> In this work, we found that CCP induces stronger N-specific humoral responses that were associated with improved clinical outcomes. This suggests that N immunodominance may be a mechanism to attenuate inflammatory activity of N-specific immune complexes in the lung while allowing the rest of the immune system to control and clear the infection. N Ab function in addition to binding is

important for the effects we see with CCP. Of the 19 N-specific Ab features that were associated with CCP treatment, the two most strongly associated with clinical benefits were ADCD and FcR2B binding. The long-lasting immunodominance shift associated with CCP treatment identified in this work highlights the potential importance of clearing N-immune complexes early in severe COVID-19 and suggests that N could be a unique target for mAb therapies modifying severe COVID-19.

The observed immunodominance shifts associated with CCP treatment were linked to improved clinical outcomes. Using orthogonal analytical approaches, we found that the diminished S features and enhanced N features in CCP-treated individuals were associated with better outcomes in control as well as in CCP-treated participants. Our data suggest that the benefits of CCP in hospitalized patients with COVID-19 may not only be due to neutralizing Ab but also shifting immunodominance of CCP recipients' immune response via Ab functional activity. This observed immunomodulatory effect suggests that passive polyclonal Ab therapy may have distinct benefits in patients with COVID-19 compared with anti-RBD mAbs and antiviral agents such as nirmatrelvir/ritonavir<sup>55</sup> and molnupiravir,<sup>56</sup> both of which target viral invasion/replication to provide clinical benefits. Most anti-RBD monoclonal agents are not designed to be immunomodulatory and likely contribute to control of infection by limiting viral spread. Thus, monoclonal capture of the virus may limit the inflammatory properties of the virus but not temper host-driven inflammation. Even sotrovimab, a newer-generation IgG1 anti-RBD Ab with a half-life extending LS mutation (M428L/N434S), is decorated with the same Fc glycans as standard monoclonal agents<sup>57,58</sup> and likely mediates protection via a similar mechanism of action. The continued evolution of new variants of concern (VOCs), most recently Omicron, has led to loss of activity for many of the RBD-targeted mAbs.<sup>59–62</sup> Polyclonal Ab therapies such as CCP, hybrid convalescent/vaccinated plasma,<sup>15</sup> COVID-19 hyperimmunoglobulin,<sup>63</sup> equine COVID-19 hyperimmunoglobulin, and transchromic COVID-19 hyperimmunoglobulin such as SAB-185<sup>64</sup> may contain the breadth of Abs needed to combat perpetually evolving pathogens by targeting multiple epitopes to bind, clear, and attenuate inflammation.

The emergence of the omicron variant has rendered most of our mAb therapeutic agents inactive.<sup>59–62</sup> As a result, there is a renewed interest in use of polyclonal Ab therapies like CCP. This class of Ab therapeutic agents is less likely to lose efficacy to new variants because it targets multiple sites in the virus, and plasma from survivors of recently circulating variants can be procured relatively quickly. By using a systematic approach in our study of the factors contributing to the therapeutic benefits of CCP, we found untapped targets for future severe COVID-19-modifying treatments. Our findings contribute to a burgeoning literature showing the promise of anti-N mAbs as a disease-modifying treatment for severe COVID-19-induced hyperinflammation. Identifying biomarkers that will predict who will respond to a passive Ab therapy like CCP will be essential to streamline COVID-19 therapy and improve outcomes. Our findings show that, by choosing CCP based on high S titers alone and selecting patients based on low pre-existing S titers, we are likely incorrectly matching patients with therapies. Finally, our research

confirms the importance of the functional S and N Ab response in treatment of COVID-19 and should guide development of COVID-19 mAb and polyclonal Ab therapeutic agents that focus not only on neutralization but also on Fc-directed functionality.

### Limitations of the study

In this work, we studied a randomized control clinical trial of hospitalized patients with severe COVID-19 where CCP treatment led to a significant decrease in mortality and improvement in disease severity. Although the UPenn CCP2 trial enrolled fewer participants than multicenter CCP trials, it used local, single-sourced plasma, which may in part explain its positive results.<sup>65</sup> By focusing our analysis on this single center, we were able to use time-to-event analysis as part of the CSC and help us better parse out the continuum of COVID-19 outcomes. Designed as a randomized trial that compared CCP with standard of care treatment, our analysis of the UPenn CCP2 trial cannot rule out the effects of non-Ab proteins present in CCP. However, Sullivan et al.<sup>9</sup> found that CCP reduced the risk of hospitalization in a trial of CCP vs. fresh-frozen plasma (FFP), suggesting that serum proteins present in FFP and CCP are not responsible for the clinical benefits found in their and our trial. We were not able to seek CCP-specific Ab features that drove COVID-19 clinical outcomes because the majority of participants in our clinical trial received CCP from two separate plasma donors. It is important to note that this study was conducted before there was widespread vaccination in the United States; we do not know how vaccination status will affect CCP response. Because the majority of participants in this study were already being treated with corticosteroids and remdesivir, we cannot address whether the activity of CCP we found here is independent or contingent on combination treatment. Despite these limitations, we were able to use deep humoral immune profiling to understand how CCP modulates host immunodominance and affects clinical outcomes.

### STAR★METHODS

Detailed methods are provided in the online version of this paper and include the following:

- **KEY RESOURCES TABLE**
- **RESOURCE AVAILABILITY**
  - Lead contact
  - Materials availability
  - Data and code availability
- **EXPERIMENTAL MODEL AND SUBJECT DETAILS**
  - Clinical studies and human serum samples
  - Primary immune cells
  - Cell lines
- **METHOD DETAILS**
  - Antibody titer and Fc-receptor binding assays
  - Ab-directed functional assays
  - Fc glycan analysis
- **QUANTIFICATION AND STATISTICAL ANALYSIS**
  - Data pre-processing
  - Visualization
  - Polar plots
  - Multivariate models

- Network analysis
- Mixed linear model
- Likelihood ratio test
- Discriminant analysis in Day60

#### SUPPLEMENTAL INFORMATION

Supplemental information can be found online at <https://doi.org/10.1016/j.xcrm.2022.100811>.

#### ACKNOWLEDGMENTS

We thank Nancy Zimmerman, Mark and Lisa Schwartz, an anonymous donor (financial support), Terry and Susan Ragon, and the SAMANA Kay MGH Research Scholars award for support. We acknowledge support from the Ragon Institute of MGH, MIT and Harvard; the Massachusetts Consortium on Pathogen Readiness (MassCPR); the NIH (3R37AI080289-11S1, R01AI146785, U19AI42790-01, U19AI135995-02, U19AI42790-01, 1U01CA260476-01, CIV-IC75N93019C00052, T32 AI007061, and 3UL1TR002556); the Gates Foundation and the Global Health Vaccine Accelerator Platform (OPP1146996 and INV-001650); and the Musk Foundation.

#### AUTHOR CONTRIBUTIONS

J.D.H., H.Y., L.-a.P., B.D.J., D.L., K.J.B., and G.A. conceived the idea. K.J.B., P.A.S., G.H.C., P.T., D.S., and I.F. designed, conducted, and analyzed the results of the randomized clinical trial. J.D.H. and G.A. designed the experiments. J.D.H., J.S.B., Y.Z., H.C., J.K., R.M., and S.S. performed the antibody profiling experiments. J.D.H., C.W., D.L., and G.A. analyzed the data. J.D.H., C.W., K.J.B., D.L., and G.A. wrote the paper with input from all authors.

#### DECLARATION OF INTERESTS

G.A. is a founder of SeromYx Systems, Inc., an equity holder in Leyden Labs, and a member of the scientific advisory board of Sanofi Pasteur.

#### INCLUSION AND DIVERSITY

We support inclusive, diverse, and equitable conduct of research.

Received: February 24, 2022

Revised: June 22, 2022

Accepted: October 16, 2022

Published: October 24, 2022

#### REFERENCES

1. Dong, E., Du, H., and Gardner, L. (2020). An interactive web-based dashboard to track COVID-19 in real time. *Lancet Infect. Dis.* 20, 533–534. [https://doi.org/10.1016/s1473-3099\(20\)30120-1](https://doi.org/10.1016/s1473-3099(20)30120-1).
2. Casadevall, A., and Pirofski, L.-a. (2020). The convalescent sera option for containing COVID-19. *J. Clin. Invest.* 130, 1545–1548. <https://doi.org/10.1172/jci138003>.
3. Libster, R., Pérez Marc, G., Wappner, D., Coviello, S., Bianchi, A., Braem, V., Esteban, I., Caballero, M.T., Wood, C., Berrueta, M., et al. (2021). Early high-titer plasma therapy to prevent severe covid-19 in older adults. *N. Engl. J. Med.* 384, 610–618. <https://doi.org/10.1056/nejmoa2033700>.
4. Joyner, M.J., Carter, R.E., Senefeld, J.W., Klassen, S.A., Mills, J.R., Johnson, P.W., Theel, E.S., Wiggins, C.C., Bruno, K.A., Klompas, A.M., et al. (2021). Convalescent plasma antibody levels and the risk of death from covid-19. *N. Engl. J. Med.* 384, 1015–1027. <https://doi.org/10.1056/nejmoa2031893>.
5. O'Donnell, M.R., Grinsztejn, B., Cummings, M.J., Justman, J.E., Lamb, M.R., Eckhardt, C.M., Philip, N.M., Cheung, Y.K., Gupta, V., João, E., et al. (2021). A randomized double-blind controlled trial of convalescent plasma in adults with severe COVID-19. *J. Clin. Invest.* 131, 150646. <https://doi.org/10.1172/jci150646>.
6. Yoon, H.A., Bartash, R., Gendlina, I., Rivera, J., Nakouzi, A., Ili, R.H.B., Wirchnianski, A.S., Paroder, M., Fehn, K., Serrano-Rahman, L., et al. (2021). Treatment of severe COVID-19 with convalescent plasma in bronx, NYC. *JCI Insight* 6, e142270. <https://doi.org/10.1172/jci.insight.142270>.
7. Avendaño-Solá, C., Ramos-Martínez, A., Muñoz-Rubio, E., Ruiz-Antorán, B., Malo de Molina, R., Torres, F., Fernández-Cruz, A., Calderón-Parra, J., Payares-Herrera, C., Díaz de Santiago, A., et al. (2021). A multicenter randomized open-label clinical trial for convalescent plasma in patients hospitalized with COVID-19 pneumonia. *J. Clin. Invest.* 131, e152740. <https://doi.org/10.1172/jci152740>.
8. Salazar, E., Christensen, P.A., Graviss, E.A., Nguyen, D.T., Castillo, B., Chen, J., Lopez, B.V., Eagar, T.N., Yi, X., Zhao, P., et al. (2021). Significantly decreased mortality in a large cohort of coronavirus disease 2019 (COVID-19) patients transfused early with convalescent plasma containing high-titer anti-severe acute respiratory syndrome coronavirus 2 (SARS-CoV-2) spike protein IgG. *Am. J. Pathol.* 191, 90–107. <https://doi.org/10.1016/j.ajpath.2020.10.008>.
9. Sullivan, D.J., Gebo, K.A., Shoham, S., Bloch, E.M., Lau, B., Shenoy, A.G., Mosnaim, G.S., Gniadek, T.J., Fukuta, Y., Patel, B., et al. (2021). Randomized controlled trial of early outpatient COVID-19 treatment with high-titer convalescent plasma. Preprint at medRxiv. <https://doi.org/10.1101/2021.12.10.21267485>.
10. The RECOVERY Collaborative Group; Horby, P.W., Estcourt, L., Peto, L., Emberson, J.R., Staplin, N., Spata, E., Pessoa-Amorim, G., Campbell, M., Roddick, A., et al. Convalescent Plasma in Patients Admitted to Hospital with COVID-19 (RECOVERY): A Randomised, Controlled, Open-Label, Platform Trial. Preprint at medRxiv. <https://doi.org/10.1101/2021.03.09.21252736>.
11. Writing Committee for the REMAP-CAP Investigators; Abdelhady, H., Abdelrazik, M., Abdi, Z., Abdo, D., Abdulle, A., Abel, L., Abouzeenni, S., Abrahamson, G., Abusamra, Y., et al. (2021). Effect of convalescent plasma on organ support-free days in critically ill patients with COVID-19. *JAMA* 326, 1690–1702. <https://doi.org/10.1001/jama.2021.18178>.
12. Bégin, P., Callum, J., Jamula, E., Cook, R., Hedde, N.M., Tinmouth, A., Zeller, M.P., Beaudoin-Bussièrès, G., Amorim, L., Bazin, R., et al. (2021). Convalescent plasma for hospitalized patients with COVID-19: an open-label, randomized controlled trial. *Nat. Med.* 27, 2012–2024. <https://doi.org/10.1038/s41591-021-01488-2>.
13. Herman, J.D., Wang, C., Loos, C., Yoon, H., Rivera, J., Eugenia Dieterle, M., Haslwanter, D., Jangra, R.K., Bortz, R.H., Bar, K.J., et al. (2021). Functional convalescent plasma antibodies and pre-infusion titers shape the early severe COVID-19 immune response. *Nat. Commun.* 12, 6853. <https://doi.org/10.1038/s41467-021-27201-y>.
14. Bar, K.J., Shaw, P.A., Choi, G.H., Aquí, N., Fesnak, A., Yang, J.B., Soto-Calderon, H., Grajales, L., Starr, J., Andronov, M., et al. (2021). A randomized controlled study of convalescent plasma for individuals hospitalized with COVID-19 pneumonia. *J. Clin. Invest.* 131, e155114. <https://doi.org/10.1172/jci155114>.
15. Focosi, D., Franchini, M., Joyner, M.J., and Casadevall, A. (2021). Comparative analysis of antibody responses from COVID-19 convalescents receiving various vaccines reveals consistent high neutralizing activity for SARS-CoV-2 variant of concern omicron. Preprint at medRxiv. <https://doi.org/10.1101/2021.12.24.21268317>.
16. Schmidt, F., Muecksch, F., Weisblum, Y., Da Silva, J., Bednarski, E., Cho, A., Wang, Z., Gaebler, C., Caskey, M., Nussenzweig, M.C., et al. (2022). Plasma neutralization of the SARS-CoV-2 omicron variant. *N. Engl. J. Med.* 386, 599–601. <https://doi.org/10.1056/nejmc2119641>.
17. O'Connell, D.; U.S. Drug and Food Administration (2021). Convalescent Plasma EUA Letter of Authorization. 12282021.
18. Wang, X., Guo, X., Xin, Q., Pan, Y., Hu, Y., Li, J., Chu, Y., Feng, Y., and Wang, Q. (2020). Neutralizing antibodies responses to SARS-CoV-2 in

- COVID-19 inpatients and convalescent patients. *Clin. Infect. Dis.* 71, ciaa721. <https://doi.org/10.1093/cid/ciaa721>.
19. Natarajan, H., Crowley, A.R., Butler, S.E., Xu, S., Weiner, J.A., Bloch, E.M., Littlefield, K., Wieland-Alter, W., Connor, R.I., Wright, P.F., et al. (2021). Markers of polyfunctional SARS-CoV-2 antibodies in convalescent plasma. *mBio* 12, 007655–e821. <https://doi.org/10.1128/mbio.00765-21>.
  20. Morgenlander, W.R., Henson, S.N., Monaco, D.R., Chen, A., Littlefield, K., Bloch, E.M., Fujimura, E., Ruczinski, I., Crowley, A.R., Natarajan, H., et al. (2021). Antibody responses to endemic coronaviruses modulate COVID-19 convalescent plasma functionality. *J. Clin. Invest.* 131, 146927. <https://doi.org/10.1172/jci146927>.
  21. Shaw, P.A., and Fay, M.P. (2016). A rank test for bivariate time-to-event outcomes when one event is a surrogate. *Stat. Med.* 35, 3413–3423. <https://doi.org/10.1002/sim.6950>.
  22. Chung, A.W., Kumar, M.P., Arnold, K.B., Yu, W.H., Schoen, M.K., Dunphy, L.J., Suscovich, T.J., Frahm, N., Linde, C., Mahan, A.E., et al. (2015). Dissecting polyclonal vaccine-induced humoral immunity against HIV using systems serology. *Cell* 163, 988–998. <https://doi.org/10.1016/j.cell.2015.10.027>.
  23. Zohar, T., Loos, C., Fischinger, S., Atyeo, C., Wang, C., Slein, M.D., Burke, J., Yu, J., Feldman, J., Hauser, B.M., et al. (2020). Compromised humoral functional evolution tracks with SARS-CoV-2 mortality. *Cell* 183, 1508–1519.e12. <https://doi.org/10.1016/j.cell.2020.10.052>.
  24. Zervou, F.N., Louie, P., Stachel, A., Zacharioudakis, I.M., Ortiz-Mendez, Y., Thomas, K., and Agüero-Rosenfeld, M.E. (2021). SARS-CoV-2 antibodies: IgA correlates with severity of disease in early COVID-19 infection. *J. Med. Virol.* 93, 5409–5415. <https://doi.org/10.1002/jmv.27058>.
  25. Bartsch, Y.C., Wang, C., Zohar, T., Fischinger, S., Atyeo, C., Burke, J.S., Kang, J., Edlow, A.G., Fasano, A., Baden, L.R., et al. (2021). Humoral signatures of protective and pathological SARS-CoV-2 infection in children. *Nat. Med.* 27, 454–462. <https://doi.org/10.1038/s41591-021-01263-3>.
  26. Ma, H., Zeng, W., He, H., Zhao, D., Jiang, D., Zhou, P., Cheng, L., Li, Y., Ma, X., and Jin, T. (2020). Serum IgA, IgM, and IgG responses in COVID-19. *Cell. Mol. Immunol.* 17, 773–775. <https://doi.org/10.1038/s41423-020-0474-z>.
  27. Yu, H.-q., Sun, B.-q., Fang, Z.-f., Zhao, J.-c., Liu, X.-y., Li, Y.-m., Sun, X.-z., Liang, H.-f., Zhong, B., Huang, Z.-f., et al. (2020). Distinct features of SARS-CoV-2-specific IgA response in COVID-19 patients. *Eur. Respir. J.* 56, 2001526. <https://doi.org/10.1183/13993003.01526-2020>.
  28. Centers for Disease Control and Prevention (2021). Science Brief: Evidence Used to Update the List of Underlying Medical Conditions Associated with Higher Risk for Severe COVID-19. [https://www.cdc.gov/coronavirus/2019-ncov/science/science-briefs/underlying-evidence-table.html?CDC\\_AA\\_refVal=https%3A%2F%2Fwww.cdc.gov%2Fcoronavirus%2F2019-ncov%2Fhcp%2Fclinical-care%2Funderlying-evidence-table.html#anchor\\_1616780486662](https://www.cdc.gov/coronavirus/2019-ncov/science/science-briefs/underlying-evidence-table.html?CDC_AA_refVal=https%3A%2F%2Fwww.cdc.gov%2Fcoronavirus%2F2019-ncov%2Fhcp%2Fclinical-care%2Funderlying-evidence-table.html#anchor_1616780486662).
  29. Frasca, D., Diaz, A., Romero, M., and Blomberg, B.B. (2017). Ageing and obesity similarly impair antibody responses. *Clin. Exp. Immunol.* 187, 64–70. <https://doi.org/10.1111/cei.12824>.
  30. Herman, J.D., Wang, C., Loos, C., Yoon, H., Rivera, J., Dieterle, M.E., Haslwanter, D., Jangra, R.K., Bortz, R.H., Bar, K.J., et al. (2021). Functional antibodies in COVID-19 convalescent plasma. Preprint at medRxiv. <https://doi.org/10.1101/2021.03.08.21253157>.
  31. Weinreich, D.M., Sivapalasingam, S., Norton, T., Ali, S., Gao, H., Bhore, R., Musser, B.J., Soo, Y., Rofail, D., Im, J., et al. (2021). REGN-COV2, a neutralizing antibody cocktail, in outpatients with covid-19. *N. Engl. J. Med.* 384, 238–251. <https://doi.org/10.1056/nejmoa2035002>.
  32. Peluso, M.J., Takahashi, S., Hakim, J., Kelly, J.D., Torres, L., Iyer, N.S., Turcios, K., Janson, O., Munter, S.E., Thanh, C., et al. (2021). SARS-CoV-2 antibody magnitude and detectability are driven by disease severity, timing, and assay. *Sci. Adv.* 7, eabh3409. <https://doi.org/10.1126/sciadv.abh3409>.
  33. Hansen, C.B., Jarhelt, I., Pérez-Alós, L., Hummelshøj Landsy, L., Loftager, M., Rosbjerg, A., Helgstrand, C., Bjelke, J.R., Egebjerg, T., Jardine, J.G., et al. (2020). SARS-CoV-2 antibody responses are correlated to disease severity in COVID-19 convalescent individuals. *J. Immunol.* 206, 109–117. <https://doi.org/10.4049/jimmunol.2000898>.
  34. Garcia-Beltran, W.F., Lam, E.C., Astudillo, M.G., Yang, D., Miller, T.E., Feldman, J., Hauser, B.M., Caradonna, T.M., Clayton, K.L., Nitido, A.D., et al. (2021). COVID-19-neutralizing antibodies predict disease severity and survival. *Cell* 184, 476–488.e11. <https://doi.org/10.1016/j.cell.2020.12.015>.
  35. Koleba, T., and Ensom, M.H.H. (2006). Pharmacokinetics of intravenous immunoglobulin: a systematic review. *Pharmacotherapy* 26, 813–827. <https://doi.org/10.1592/phco.26.6.813>.
  36. Arnold, J.N., Wormald, M.R., Sim, R.B., Rudd, P.M., and Dwek, R.A. (2007). The impact of glycosylation on the biological function and structure of human immunoglobulins. *Annu. Rev. Immunol.* 25, 21–50. <https://doi.org/10.1146/annurev.immunol.25.022106.141702>.
  37. Raju, T.S. (2008). Terminal sugars of Fc glycans influence antibody effector functions of IgGs. *Curr. Opin. Immunol.* 20, 471–478. <https://doi.org/10.1016/j.coi.2008.06.007>.
  38. Jennewein, M.F., and Alter, G. (2017). The immunoregulatory roles of antibody glycosylation. *Trends Immunol.* 38, 358–372. <https://doi.org/10.1016/j.it.2017.02.004>.
  39. Larsen, M.D., de Graaf, E.L., Sonneveld, M.E., Plomp, H.R., Nouta, J., Hoepel, W., Chen, H.-J., Linty, F., Visser, R., Brinkhaus, M., et al. (2021). Afucosylated IgG characterizes enveloped viral responses and correlates with COVID-19 severity. *Science* 371, eabc8378. <https://doi.org/10.1126/science.abc8378>.
  40. Chakraborty, S., Gonzalez, J., Edwards, K., Mallajosyula, V., Buzzanco, A.S., Sherwood, R., Buffone, C., Kathale, N., Providenza, S., Xie, M.M., et al. (2020). Proinflammatory IgG Fc structures in patients with severe COVID-19. *Nat. Immunol.* 22, 67–73. <https://doi.org/10.1038/s41590-020-00828-7>.
  41. Kaneko, Y., Nimmerjahn, F., and Ravetch, J.V. (2006). Anti-inflammatory activity of immunoglobulin G resulting from Fc sialylation. *Science* 313, 670–673. <https://doi.org/10.1126/science.1129594>.
  42. Anthony, R.M., Nimmerjahn, F., Ashline, D.J., Reinhold, V.N., Paulson, J.C., and Ravetch, J.V. (2008). Recapitulation of IVIG anti-inflammatory activity with a recombinant IgG Fc. *Science* 320, 373–376. <https://doi.org/10.1126/science.1154315>.
  43. Karsten, C.M., Pandey, M.K., Figge, J., Kilchenstein, R., Taylor, P.R., Rosas, M., McDonald, J.U., Orr, S.J., Berger, M., Petzold, D., et al. (2012). Anti-inflammatory activity of IgG1 mediated by Fc galactosylation and association of FcγRIIB and dectin-1. *Nat. Med.* 18, 1401–1406. <https://doi.org/10.1038/nm.2862>.
  44. Hoepel, W., Chen, H.-J., Geyer, C.E., Allahverdiyeva, S., Manz, X.D., de Taeye, S.W., Aman, J., Mes, L., Steenhuis, M., Griffith, G.R., et al. (2021). High titers and low fucosylation of early human anti-SARS-CoV-2 IgG promote inflammation by alveolar macrophages. *Sci. Transl. Med.* 13, eabf8654. <https://doi.org/10.1126/scitranslmed.abf8654>.
  45. Zhou, Y., Fu, B., Zheng, X., Wang, D., Zhao, C., Qi, Y., Sun, R., Tian, Z., Xu, X., and Wei, H. (2020). Pathogenic T-cells and inflammatory monocytes incite inflammatory storms in severe COVID-19 patients. *Natl. Sci. Rev.* 7, 998–1002. <https://doi.org/10.1093/nsr/nwaa041>.
  46. Grace, P.S., Dolatshahi, S., Lu, L.L., Cain, A., Palmieri, F., Petrone, L., Fortune, S.M., Ottenhoff, T.H.M., Lauffenburger, D.A., Goletti, D., et al. (2021). Antibody subclass and glycosylation shift following effective TB treatment. *Front. Immunol.* 12, 679973. <https://doi.org/10.3389/fimmu.2021.679973>.
  47. Ho, C.-H., Chien, R.-N., Cheng, P.-N., Liu, J.-H., Liu, C.-K., Su, C.-S., Wu, I.-C., Li, I.-C., Tsai, H.-W., Wu, S.-L., et al. (2015). Aberrant serum immunoglobulin G glycosylation in chronic hepatitis B is associated with histological liver damage and reversible by antiviral therapy. *J. Infect. Dis.* 211, 115–124. <https://doi.org/10.1093/infdis/jiu388>.

48. Anthony, R.M., Kobayashi, T., Wermeling, F., and Ravetch, J.V. (2011). Intravenous gammaglobulin suppresses inflammation through a novel TH2 pathway. *Nature* 475, 110–113. <https://doi.org/10.1038/nature10134>.
49. Fiebiger, B.M., Maamary, J., Pincetic, A., and Ravetch, J.V. (2015). Protection in antibody- and T cell-mediated autoimmune diseases by antiinflammatory IgG Fcs requires type II FcRs. *Proc. Natl. Acad. Sci. USA* 112, E2385–E2394. <https://doi.org/10.1073/pnas.1505292112>.
50. Bournazos, S., Corti, D., Virgin, H.W., and Ravetch, J.V. (2020). Fc-optimized antibodies elicit CD8 immunity to viral respiratory infection. *Nature* 588, 485–490. <https://doi.org/10.1038/s41586-020-2838-z>.
51. Lofano, G., Gorman, M.J., Yousif, A.S., Yu, W.-H., Fox, J.M., Dugast, A.-S., Ackerman, M.E., Suscovich, T.J., Weiner, J., Barouch, D., et al. (2018). Antigen-specific antibody Fc glycosylation enhances humoral immunity via the recruitment of complement. *Sci. Immunol.* 3, eaat7796. <https://doi.org/10.1126/sciimmunol.aat7796>.
52. Gao, T., Hu, M., Zhang, X., Li, H., Zhu, L., Liu, H., Dong, Q., Zhang, Z., Wang, Z., Hu, Y., et al. (2020). Highly pathogenic coronavirus N protein aggravates lung injury by MASP-2-mediated complement over-activation. Preprint at medRxiv. <https://doi.org/10.1101/2020.03.29.20041962>.
53. Kang, S., Yang, M., He, S., Wang, Y., Chen, X., Chen, Y.-Q., Hong, Z., Liu, J., Jiang, G., Chen, Q., et al. (2021). A SARS-CoV-2 antibody curbs viral nucleocapsid protein-induced complement hyperactivation. *Nat. Commun.* 12, 2697. <https://doi.org/10.1038/s41467-021-23036-9>.
54. Ma, L., Sahu, S.K., Cano, M., Kuppuswamy, V., Bajwa, J., McPhatter, J., Pine, A., Meizlish, M.L., Goshua, G., Chang, C.H., et al. (2021). Increased complement activation is a distinctive feature of severe SARS-CoV-2 infection. *Sci. Immunol.* 6, eabh2259. <https://doi.org/10.1126/sciimmunol.abh2259>.
55. Pfizer (2021). Pfizer Announces Additional Phase 2/3 Study Results Confirming Robust Efficacy of Novel COVID-19 Oral Antiviral Treatment Candidate in Reducing Risk of Hospitalization or Death. <https://www.pfizer.com/news/press-release/press-release-detail/pfizer-announces-additional-phase-23-study-results>.
56. Bernal, A.J., Silva, M.M.G., Musungaie, D.B., Kovalchuk, E., Gonzalez, A., Reyes, V.D., Martín-Quirós, A., Caraco, Y., Williams-Diaz, A., Brown, M.L., et al. (2021). Molnupiravir for oral treatment of covid-19 in nonhospitalized patients. *New Engl. J. Med.* NEJMoa2116044. <https://doi.org/10.1056/nejmoa2116044>.
57. Agency, E.M. (2021). CHMP assessment report: Xevudy (Committee for Medicinal Products for Human Use).
58. Raymond, C. (2011). Production of highly sialylated monoclonal antibodies. In *Glycosylation*, S. Petrescu, ed., IntechOpen. <https://doi.org/10.5772/51301>.
59. Cameroni, E., Saliba, C., Bowen, J.E., Rosen, L.E., Culp, K., Pinto, D., VanBlargan, L.A., Marco, A.D., Zepeda, S.K., Iulio, J.d., et al. (2021). Broadly neutralizing antibodies overcome SARS-CoV-2 Omicron antigenic shift. Preprint at bioRxiv. <https://doi.org/10.1101/2021.12.12.472269>.
60. Aggarwal, A., Stella, A.O., Walker, G., Akerman, A., Milogiannakis, V., Brilot, F., Amatayakul-Chantler, S., Roth, N., Coppola, G., Schofield, P., et al. (2021). SARS-CoV-2 Omicron: evasion of potent humoral responses and resistance to clinical immunotherapeutics relative to viral variants of concern. Preprint at medRxiv. <https://doi.org/10.1101/2021.12.14.21267772>.
61. Planas, D., Saunders, N., Maes, P., Guivel-Benhassine, F., Planchais, C., Buchrieser, J., Bolland, W.-H., Porrot, F., Staropoli, I., Lemoine, F., et al. (2021). Considerable escape of SARS-CoV-2 variant Omicron to antibody neutralization. Preprint at bioRxiv. <https://doi.org/10.1101/2021.12.14.472630>.
62. Cao, Y., Wang, J., Jian, F., Xiao, T., Song, W., Yisimayi, A., Huang, W., Li, Q., Wang, P., An, R., et al. (2021). Omicron escapes the majority of existing SARS-CoV-2 neutralizing antibodies. Preprint at bioRxiv. <https://doi.org/10.1101/2021.12.07.470392>.
63. Ali, S., Uddin, S.M., Shalim, E., Sayeed, M.A., Anjum, F., Saleem, F., Muhaymin, S.M., Ali, A., Ali, M.R., Ahmed, I., et al. (2021). Hyperimmune anti-COVID-19 IVIG (C-IVIG) treatment in severe and critical COVID-19 patients: a phase I/II randomized control trial. *Eclinicalmedicine* 36, 100926. <https://doi.org/10.1016/j.eclim.2021.100926>.
64. Liu, Z., Wu, H., Eglund, K.A., Gilliland, T.C., Dunn, M.D., Luke, T.C., Sullivan, E.J., Klimstra, W.B., Bausch, C.L., and Whelan, S.P.J. (2021). Human immunoglobulin from transchromosomal bovines hyperimmunized with SARS-CoV-2 spike antigen efficiently neutralizes viral variants. *Hum. Vaccines Immunother.* 18, 1940652. <https://doi.org/10.1080/21645515.2021.1940652>.
65. Kunze, K.L., Johnson, P.W., van Helmond, N., Senefeld, J.W., Petersen, M.M., Klassen, S.A., Wiggins, C.C., Klompas, A.M., Bruno, K.A., Mills, J.R., et al. (2021). Mortality in individuals treated with COVID-19 convalescent plasma varies with the geographic provenance of donors. *Nat. Commun.* 12, 4864. <https://doi.org/10.1038/s41467-021-25113-5>.
66. Boesch, A.W., Brown, E.P., Cheng, H.D., Ofori, M.O., Normandin, E., Nigrovic, P.A., Alter, G., and Ackerman, M.E. (2014). Highly parallel characterization of IgG Fc binding interactions. *mAbs* 6, 915–927. <https://doi.org/10.4161/mabs.28808>.
67. Brown, E.P., Dowell, K.G., Boesch, A.W., Normandin, E., Mahan, A.E., Chu, T., Barouch, D.H., Bailey-Kellogg, C., Alter, G., and Ackerman, M.E. (2017). Multiplexed Fc array for evaluation of antigen-specific antibody effector profiles. *J. Immunol. Methods* 443, 33–44. <https://doi.org/10.1016/j.jim.2017.01.010>.
68. Ackerman, M.E., Moldt, B., Wyatt, R.T., Dugast, A.-S., McAndrew, E., Tsoukas, S., Jost, S., Berger, C.T., Sciaranghella, G., Liu, Q., et al. (2011). A robust, high-throughput assay to determine the phagocytic activity of clinical antibody samples. *J. Immunol. Methods* 366, 8–19. <https://doi.org/10.1016/j.jim.2010.12.016>.
69. Ackerman, M.E., Das, J., Pittala, S., Broge, T., Linde, C., Suscovich, T.J., Brown, E.P., Bradley, T., Natarajan, H., Lin, S., et al. (2018). Route of immunization defines multiple mechanisms of vaccine-mediated protection against SIV. *Nat. Med.* 24, 1590–1598. <https://doi.org/10.1038/s41591-018-0161-0>.
70. Lu, L.L., Chung, A.W., Rosebrock, T.R., Ghebremichael, M., Yu, W.H., Grace, P.S., Schoen, M.K., Tafesse, F., Martin, C., Leung, V., et al. (2016). A functional role for antibodies in tuberculosis. *Cell* 167, 433–443.e14. <https://doi.org/10.1016/j.cell.2016.08.072>.
71. Fischinger, S., Fallon, J.K., Michell, A.R., Broge, T., Suscovich, T.J., Streeck, H., and Alter, G. (2019). A high-throughput, bead-based, antigen-specific assay to assess the ability of antibodies to induce complement activation. *J. Immunol. Methods* 471, 44. <https://doi.org/10.1016/j.jim.2019.07.002>.
72. Karsten, C.B., Mehta, N., Shin, S.A., Diefenbach, T.J., Slein, M.D., Karpinski, W., Irvine, E.B., Broge, T., Suscovich, T.J., and Alter, G. (2019). A versatile high-throughput assay to characterize antibody-mediated neutrophil phagocytosis. *J. Immunol. Methods* 471, 46–56. <https://doi.org/10.1016/j.jim.2019.05.006>.
73. Alter, G., Malenfant, J.M., and Altfield, M. (2004). CD107a as a functional marker for the identification of natural killer cell activity. *J. Immunol. Methods* 294, 15–22. <https://doi.org/10.1016/j.jim.2004.08.008>.
74. Colucci, F., Caligiuri, M.A., and Di Santo, J.P. (2003). What does it take to make a natural killer? *Nat. Rev. Immunol.* 3, 413–425. <https://doi.org/10.1038/nri1088>.
75. Mahan, A.E., Tedesco, J., Dionne, K., Baruah, K., Cheng, H.D., De Jager, P.L., Barouch, D.H., Suscovich, T., Ackerman, M., Crispin, M., and Alter, G. (2015). A method for high-throughput, sensitive analysis of IgG Fc and Fab glycosylation by capillary electrophoresis. *J. Immunol. Methods* 417, 34–44. <https://doi.org/10.1016/j.jim.2014.12.004>.

STAR★METHODS

KEY RESOURCES TABLE

REAGENT or RESOURCE	SOURCE	IDENTIFIER
<b>Antibodies</b>		
Mouse Anti-Human IgG1-Fc PE	Southern Biotech	CAT# 9054-09; RRID: AB_2796628
Mouse Anti-Human IgG2-Fc PE	Southern Biotech	CAT# 9060-09; RRID: AB_2796635
Mouse Anti-Human IgG3-Fc PE	Southern Biotech	CAT# 9210-09; RRID: AB_2796701
Mouse Anti-Human IgM-Fc PE	Southern Biotech	CAT# 9020-09; RRID: AB_2796577
Mouse Anti-Human IgA1-Fc PE	Southern Biotech	CAT# 9130-09; RRID: AB_2796656
Mouse Anti-Human IgA2-Fc PE	Southern Biotech	CAT# 9140-09; RRID: AB_2796664
Pacific Blue(TM) anti-human CD66b antibody	Biolegend	CAT# 305112; RRID: AB_2563294
<b>Chemicals, peptides, and recombinant proteins</b>		
SARS-CoV-2 nucleocapsid (N) protein	Aalto BioReagents	CAT# CK 6404-b
SARS-CoV-2 spike protein (S)	Lake Pharma	CAT # 46934
SARS-CoV-2 subunit 1 and 2 of the spike protein (S1 and S2)	Sino Biological	CAT#: 40591-V08B1; 40590-V08B
SARS-CoV-2 RBD domain of the spike protein	Provided by Aaron Schmidt, Ragon Institute	N/A
SARS-CoV-2 N-terminal domain (NTD) domain of the spike protein	Sino Biological	CAT#: 40591-V49H
Flu-HA proteins: H1N1/A/New Caledonia/20/99, H1N1/A/Solomon Islands/3/2006, H3N2(A/Brisbane/10/2007	Immune Tech	CAT# IT-003-001ΔTMp, IT-003-0011ΔTMp, IT-003-0042ΔTMp
Recombinant Ebola Glycoprotein-d TM	IBT Bioservices	CAT# 0501-016
Human Fc receptors	Produced at the Duke Human Vaccine Institute, <sup>66</sup>	N/A
Streptavidin-R-Phycoerythrin	Prozyme	CAT# PJ31S
EDC (1-ethyl-3-(3-dimethylaminopropyl) carbodiimide hydrochloride)	Thermo Fisher	CAT# 77149
Sulfo-NHS-LC-LC biotin	Thermo Fisher	CAT# A35358
DMTMM (4-(4,6-Dimethoxy-1,3,5-triazin-2-yl)-4-methylmorpholinium chloride)	Sigma Aldrich	74104
Lyophilized guinea pig complement	Cedarlane	CL4051
<b>Deposited data</b>		
Processed Ab Titer, Subclass, FcR-binding, Functional assay, and Fc-Glycans data	This paper; Mendeley Data	Table S5; <a href="https://doi.org/10.17632/zc5dzbn9tb.1">https://doi.org/10.17632/zc5dzbn9tb.1</a>
<b>Experimental models: Cell lines</b>		
THP-1	ATCC	ATCC: TIB-202
<b>Software and algorithms</b>		
IntelliCyt ForeCyt (v8.1)	Sartorius	<a href="https://intellicyt.com/products/software/">https://intellicyt.com/products/software/</a>
FlowJo (v10.7.1)	FlowJo, LLC	<a href="https://www.flowjo.com/solutions/flowjo">https://www.flowjo.com/solutions/flowjo</a>
Prism 9.2.0 (283)	GraphPad	<a href="https://www.graphpad.com/scientific-software/prism/">https://www.graphpad.com/scientific-software/prism/</a>
<b>Other</b>		
FluoSpheres™ NeutrAvidin™-Labeled Microspheres, 1.0 μm, yellow-green fluorescent (505/515), 1% solids	Invitrogen	CAT# F8776

(Continued on next page)

**Continued**

REAGENT or RESOURCE	SOURCE	IDENTIFIER
FluoSpheres™ Carboxylate-Modified Microspheres, 1.0 μm, blue (fluorescent 350/440), 1% solids	Invitrogen	CAT# F8815
FluoSpheres™ NeutrAvidin™-Labeled Microspheres, 1.0 μm, crimson fluorescent (625/645), 1% solids	Invitrogen	N/A
FluoSpheres™ NeutrAvidin™-Labeled Microspheres, 1.0 μm, red-orange fluorescent (565/580) 1% solids	Invitrogen	N/A
MagPlex microspheres	Luminex corporation	CAT# MC12001-01

**RESOURCE AVAILABILITY**

**Lead contact**

Further information and requests for resources and reagents should be directed to and will be fulfilled by the lead contact, Galit Alter ([galter@mgh.harvard.edu](mailto:galter@mgh.harvard.edu)).

**Materials availability**

This study did not generate new unique reagents.

**Data and code availability**

- The processed dataset generated during and analyzed during the current study have been made available in [Table S5](#) and deposited at Mendeley Data: <https://doi.org/10.17632/zc5dzbn9tb.1>. Antibody class, subclass, FcR-binding, and functional assay measurements are included in the first sheet of the table and Spike-specific Fc-glycans data is included in the second sheet.
- Custom code was used in this manuscript and has been made available at Zenodo.org: [6110200](https://zenodo.org/record/6110200). The R packages used for data analysis are described in more detail in the [STAR methods](#) section, and more information is available upon request.
- Any additional information required to reanalyze the data reported in this paper is available from the [lead contact](#) upon request.

**EXPERIMENTAL MODEL AND SUBJECT DETAILS**

**Clinical studies and human serum samples**

The cohort described here participated in a randomized control trial of convalescent plasma in hospitalized patients with severe COVID-19, as described in Bar et al.<sup>14</sup> Briefly, the study enrolled hospitalized adults with RT-PCR-confirmed SARS-CoV-2 infection, radiographic documentation of pneumonia, and abnormal respiratory status, defined as room air saturation of oxygen (SaO<sub>2</sub>) <93%, or requiring supplemental oxygen, or tachypnea with a respiratory rate ≥ 30 breaths per minute. Participants were excluded if they had a contraindication to transfusion, were participating in other clinical trials of investigational COVID-19 therapy, if there was clinical suspicion that the etiology of acute illness was primarily due to a condition other than COVID-19, or if ABO-compatible CCP was unavailable. Between May 2020 and January 2021, a total of 80 eligible participants were randomized to receive either 2 units of CCP and standard of care (treatment arm) versus standard of care alone (control arm). Participants were assigned to treatment or control in a 1:1 ratio. 41 participants were randomized to treatment, but two declined CCP administration and 40 were included in our analysis; 39 participants were randomized to control. 39 participants in the treatment arm received up to 2 units of convalescent plasma on study day 1; with 4 participants receiving 2 units from the same donor and 35 receiving units from two distinct donors. Participants were enrolled a median of 6 days (IQR 4–9) after the onset of COVID-19 symptoms. None of the participants were on mechanical ventilation on enrollment. The majority of participants received steroids (83%) and remdesivir (81%) at enrollment. The median age of participants was 63 (IQR 52–74), and 41% had diabetes, 67% had hypertension, 45% had obesity, 32% had chronic kidney disease, 27% had cancer, and 14% had immunodeficiencies. Of the enrolled participants, 54% were female and 45% were male. The majority of participants identified as African American (53%), with 5% identifying as Asian, 4% identifying as Latino/a, 34% identifying as Non-Latino/a Caucasian, and 4% without an identified race or ethnicity.

The clinical cohort described in Bar et al.<sup>14</sup> was approved by the University of Pennsylvania institutional review board and registered at [ClinicalTrials.gov](https://clinicaltrials.gov) with number NCT04397757. All participants provided informed consent prior to participation in the study. Secondary Use of patient samples and clinical samples was approved by the Mass General Brigham Institutional Review Board.

## Primary immune cells

Fresh peripheral blood was collected by the MGH Blood bank from healthy human volunteers. All volunteers gave signed consent and were over 18 years of age, and all samples were de-identified before use. The study was approved by the MGH Institutional Review Board. Human neutrophils were isolated from fresh peripheral blood and maintained at 37°C, 5% CO<sub>2</sub> in RPMI with 10% fetal bovine serum, L-glutamine, penicillin/streptomycin.

## Cell lines

THP-1 cells (ATCC), a monocytic leukemia cell line, were maintained in RPMI supplemented with 10% fetal bovine serum, L-glutamine, penicillin/streptomycin, HEPES, and beta-mercaptoethanol. THP-1 cells were grown at 37°C, 5% CO<sub>2</sub>.

## METHOD DETAILS

### Antibody titer and Fc-receptor binding assays

Antigen-specific antibody subclass, isotype, and Fc-receptor (FcR) binding levels were assayed with a customized multiplexed Luminex bead array, as previously described.<sup>67</sup> This allowed for relative quantification of antigen-specific humoral responses in a high-throughput manner and simultaneous detection of many antigens. A panel of SARS-CoV-2 antigens including the full spike glycoprotein (S) (provided by Lake Pharma), receptor binding domain (RBD) (Provided by Aaron Schmidt, Ragon Institute) nucleocapsid (N) (Aalto Bio Reagents, Dublin, Ireland), S1 (Sino Biological, Beijing, China) S2 (Sino Biological, Beijing, China), and N-terminal domain (NTD) (Sino Biological, Beijing, China) were used. Control antigens were run including a mix of three Flu-HA proteins (H1N1/A/New Caledonia/20/99, H1N1/A/Solomon Islands/3/2006, H3N2)(A/Brisbane/10/2007 – Immune Tech) and Ebola glycoprotein (IBT Bioservices). In brief, antigens were coupled to uniquely fluorescent magnetic carboxyl-modified microspheres (Luminex Corporation, Austin, TX) using 1-Ethyl-3-(3-dimethylaminopropyl) carbodiimide (EDC) (Thermo Fisher Scientific, Waltham, MA) and Sulfo-N-hydroxysuccinimide (NHS) (Thermo Fisher Scientific, Waltham, MA). Antigen-coupled microspheres were then blocked, washed, and incubated for 16 h at 4°C while rocking at 700 rpm with diluted plasma samples at plate concentrations of 1:12,000 for all subclasses and isotypes and C1q and FcRn binding and 1:120,000 for all other Fc-receptors to form immune complexes in a 20  $\mu$ L volume in 384-well plates (Greiner, Monroe, NC). The following day, plates were washed using an automated plate washer (Tecan, Männedorf, Zürich, Switzerland) with 0.1% BSA and 0.02% Tween 20. Antigen-specific antibody titers were detected with Phycoerythrin (PE)-coupled antibodies against IgG1, IgG2, IgG3, IgG4, IgA1, and IgM (SouthernBiotech, Birmingham, AL). To measure antigen-specific Fc-receptor binding, biotinylated Fc-receptors (FcR2AH, 2B, 3AV, 3B, FcRn, FCAR, FCR3AV – Duke Protein Production facility, C1q – Sigma Aldrich) were coupled to PE to form tetramers and then added to immune-complexed beads to incubate for 1 h at room temperature while shaking. Fluorescence was detected using an Intellicyt iQue with a 384-well plate handling robot (PAA) and analyzed using Forecyt software by gating on fluorescent bead regions. PE median fluorescence intensity (MFI) was measured as the readout of each antigen-specific antibody measurements. All experiments were performed in duplicate while operators were blinded to study group assignment and all cases and controls were run at the same time to avoid batch effects. The mean value of the duplicate measurements was used for further statistical analysis.

### Ab-directed functional assays

Bead-based assays were used to quantify antibody-dependent cellular phagocytosis (ADCP), antibody-dependent neutrophil phagocytosis (ADNP) and antibody-dependent complement deposition (ADCD), as previously described.<sup>68–72</sup> Yellow (ADNP and ADCD) as well as red (ADCD) fluorescent neutravadin beads (Thermo Fisher) were coupled to biotinylated SARS-CoV-2 S antigens and incubated with diluted plasma (ADCP 1:100, ADNP 1:50, ADCD 1:10) to allow immune complex formation for 2 h at 37°C. To assess the ability of sample antibodies to induce monocyte phagocytosis, THP-1s (ATCC) were added to the immune complexes at 1.25E5cells/ml and incubated for 16 h at 37°C. For ADNP, primary neutrophils were isolated via negative selection (Stemcell) from whole blood. Isolated neutrophils at a concentration of 50,000 per well were incubated with immune complexes for 1 h incubation at 37°C. Neutrophils were stained with an anti-CD66b PacBlue detection antibody (Biolegend) and fixed with 4% paraformaldehyde (Alfa Aesar). To measure antibody-dependent deposition of C3, lyophilized guinea pig complement (Cedarlane) was reconstituted according to manufacturer's instructions and diluted in gelatin veronal buffer with calcium and magnesium (GBV++) (Boston BioProducts) and mixed with immune complexes. After a 20-min incubation at 37°C, C3 was detected with an anti-C3 fluorescein-conjugated goat IgG fraction detection antibody (Mpbio). Antibody-dependent NK (ADNK) cell activity was measured via an ELISA-based assay, as described previously (Chung et al., 2015). Briefly, plates were coated with 3 mg/mL of antigen (SARS-CoV-2 S) and blocked overnight at 4°C. NK cells were isolated the day of the assay with negative selection (RosetteSep – Stem Cell Technologies) from healthy buffy coats (MGH blood donor center). Diluted plasma samples were added to the antigen-coated plates (1:25 dilution) and incubated for 2 h at 37°C. NK cells were mixed with a staining cocktail containing anti-CD107a BV605 antibody (Biolegend), Golgi stop (BD Biosciences) and Brefeldin A (BFA, Sigma Aldrich).  $2.5 \times 10^5$  cells/ml were added per well to the immune complexes and incubated for 5 h at 37°C. Next, cells were fixed (Perm A, Invitrogen) and stained for surface markers with anti-CD3 APC-Cy7 (BioLegend) and anti-CD56 PE-Cy7 (BD Biosciences). Subsequently, cells were permeabilized using Perm B (Invitrogen) and intracellularly stained with an anti-MIP-1 $\beta$ -BV421 (BD Biosciences) and IFN $\gamma$ -PE (BioLegend) antibodies.

All assays were acquired via flow cytometry with iQue (Intellicyt) and an S-Lab 384-well plate handling robot (PAA). For ADCP, events were gated on singlets and bead-positive cells. For ADNP, neutrophils were defined as CD66b positive events followed by gating on bead-positive neutrophils. A phagocytosis score was calculated for ADCP and ADNP as (percentage of bead-positive cells) x (MFI of bead-positive cells) divided by 10,000. For ADCD, complement deposition was reported as the median fluorescence intensity of C3 deposition on Spike-coupled beads. For ADNK, NK cells were defined as CD3<sup>-</sup> and CD56<sup>+</sup> events. NK cell activation was quantified as the percentage of NK cells positive for the degranulation marker CD107a<sup>73</sup> and for two markers of NK cell activation, MIP-1 $\beta$ , and IFN $\gamma$ .<sup>74</sup> In the text, we referred to these readouts as CD107aNK, MIP-1 $\beta$ NK, and IFN $\gamma$ NK.

### Fc glycan analysis

Capillary electrophoresis was conducted as previously described.<sup>75</sup> Briefly, recombinant S was biotinylated and coupled to 1  $\mu$ m neutravidin-coated magnetic beads; 5  $\mu$ g of protein was coupled to 50  $\mu$ L of beads for each sample. Heat-inactivated sample (100  $\mu$ L) was incubated with 50  $\mu$ L of un-coupled magnetic beads to clear non-specific bead binding for 30 min. Pre-cleared plasma was incubated with 50  $\mu$ L of protein-coupled beads and incubated for 1 h at 37°C, were washed, and the captured antibody Fc was cleaved off by incubating with 1  $\mu$ L of IDEZ at 37°C for 1 h. The isolated Fc fragments were deglycosylated and the freed glycans were fluorescently labeled and purified using a GlycanAssure APTS Kit according to the manufacturer's instructions. Glycans were analyzed by capillary electrophoresis on 3500xL genetic analyzer (Applied Biosystems). Samples were run with N-glycan fucosyl, afucosyl, bisecting and mannose N-glycan libraries to enable identification of twenty-two discrete glycan species. Glycan profiles of each labeled and purified participant sample was measured with technical duplicate. The relative frequencies of each glycan peak were plotted as a percentage of total glycans, calculated using GlycanAssure software.

## QUANTIFICATION AND STATISTICAL ANALYSIS

### Data pre-processing

Duplicate measurements of antibody isotypes, subclasses, FcR-binding levels and ADCD measurements were averaged for each sample and then log<sub>10</sub> transformed. Duplicate measurements of ADNK, ADCP, and ADNP were averaged for each sample. In order to remove antibody features with low magnitude signals, we used the variation in the control samples as a cut off. More specifically, we removed antibody features whose maximum signal in the CCP recipients was less than four standard deviations over the negative control PBS wells (Mean PBS + 4x PBS SD).

### Visualization

The heatmaps were created with the function `pheatmap` in R package 'pheatmap' (version 1.0.12). To eliminate the effect of extreme values and visualize the predominant differences clearly, the color ranges were equally divided into 100 intervals by the quantile range of the percentage of adjusted values across all the measurements. The UMAP visualization was performed on principal components whose cumulative explained variance is larger than 90% by `umap` function in R package 'umap' (version 0.2.7.0) with fine-tuning parameters (`neighbor = 8`, `min.dist = 0.1`), and visualized by `ggplot` function in R package `ggplot2` (version 3.3.5).

### Polar plots

Polar plots were used to visualize the mean percentile of groups in Figures 2C, 3C, and 5A. Percentile rank scores were determined for each feature across all considered samples using the function 'percent\_rank' of the R package 'dplyr' (version 1.0.5).

Polar plots for Figure S1C were used to visualize the S-specific individual antibody profile of CCP-treated and control participants over the course of the clinical trial. Each feature across the respective populations was scaled by min-max normalization.

### Multivariate models

#### Four parameters logistic regression model

The details of four parameters logistic regression model were explained in our previous paper.<sup>23</sup> Briefly, all the measurements were normalized to make sure the minimal values across groups were zero and the maximum values were one. To determine the difference of fitted models in each antibody feature involved in the control and treatment groups, the dynamics along the days since symptom onset were described in each group (CCP-treated and control) at the population level using a four-parameter logistic growth curve. Furthermore, to detect differences explained by different explicit parameters between control and CCP-treatment group, we built two paired models simultaneously, allowing for combinations of parameters to differ between the two groups, while the others are shared between the groups. 16 models controlled by the combination of four parameters were evaluated by Akaike Information Criterion (AIC) to balance the model fitness and model complexity. Finally, the best model was picked with the lowest AIC values. Additionally, to analyze the overall difference in parameters across the groups (Figure 2E), the maximum likelihood estimates for all the models were combined by weighing the contribution of individual models by the Akaike weight.

#### Regression with clinical severity score

The regression model in Figure 2H was trained to associate Clinical Severity Score with top 30 features suggested by the four parameters logistic regression model with a minimal set of features. First, we applied the least absolute shrinkage and selection operator (LASSO) feature selection algorithm to extract significant features. Here, we run the LASSO feature selection 10 times on the

whole dataset and picked the set of features, whose occurrences are more than seven times. The details were implemented in the function 'select\_lasso' in systemseRology R package (v.1.0). Then, a partial least square regression model was trained using the Lasso-selected features. Model performance was evaluated by 5-fold cross-validation and the negative models were constructed from permuted labels with multiple iterations. The permuted control models were generated 20 times by shuffling labels randomly for each iteration. Coefficient of determination, denoted as  $R^2$  was used to evaluate the regression performance. For PLS-R, we use the 'opls' function in R package 'ropls' (v.1.22.0) for regression and functions in systemseRology R package for the purpose of visualization.

To further investigate the predicted performance of clinical severity score using the features selected by LASSO, the whole samples were divided into two groups (higher severity and lower severity) using the threshold 20. Then, the predicted clinical severity scores for all the involved samples were predicted using 5-folds cross-validation for 100 repetitions. After that, the averaged ROC curve with the roc curve from each repetition were visualized by roc function in R package pROC (version 1.18.0) as depicted in Figure 2K.

### Network analysis

The correlation networks were used to visualize the additional immune measurements significantly associated with the LASSO-selected features, indicating enhanced insights of biological mechanisms. The measurements that were significantly ( $p$  value  $<0.05$ ) correlated with the selected features after a Benjamini-Hochberg correction were defined as co-correlates. Significant spearman correlations above a threshold of  $|r| > 0.7$  were visualized within the networks. In detail, the spearman correlation coefficients were calculated using 'rcorr' function in 'Hmisc' package (v4.4.2) and the  $p$  values were corrected by "Benjamini-Hochberg" correction in 'stats' package (v.4.0.3). For the purpose of visualization, the correlation networks were visualized using 'ggraph' (v.2.0.4) and 'igraph' (v.1.2.6) packages.

### Mixed linear model

We used two nested mixed linear models (null and full model) without/with treatment group information to assess the significance of the association between measured antibody levels and treatment groups while controlling for potential confounding clinical characteristics. We fit two mixed linear models and estimated the improvement in model fit by likelihood ratio testing to identify the associated measurements for participant timepoints from the first two weeks of the trial (D1, 3, 8, and 15).

Null Model: antibodymeasurement  $\sim 1 + \text{AGE\_CAT} + \text{GENDER} + \text{RACE} + \text{ETHNICITY} + \text{POOL\_BLOOD} + \text{ENROLLQTR} + \text{TOTALCMB} + \text{DM} + \text{CVD} + \text{HTN} + \text{OBESITY} + \text{CKD} + \text{CANCER} + \text{IMMDF} + \text{CM\_RMDSVR} + \text{CM\_STERIODS} + \text{SymOnSet} + (\text{TimeGroup} | \text{Sample.ID})$ .

Full Model: antibodymeasurement  $\sim 1 + \text{CCP\_vs\_Control} + \text{AGE\_CAT} + \text{GENDER} + \text{RACE} + \text{ETHNICITY} + \text{POOL\_BLOOD} + \text{ENROLLQTR} + \text{TOTALCMB} + \text{DM} + \text{CVD} + \text{HTN} + \text{OBESITY} + \text{CKD} + \text{CANCER} + \text{IMMDF} + \text{CM\_RMDSVR} + \text{CM\_STERIODS} + \text{SymOnSet} + (\text{TimeGroup} | \text{Sample.ID})$ .

### Likelihood ratio test

$\text{LRT} = -2 * \ln(\text{MLE in Full model} / \text{MLE in Null model}) \sim \chi^2$ .

Here, the subject clinical information includes age at enrollment category, gender, race, ethnicity, blood type and enrollment period (May-Jun 2020, July-Aug 2020, Sep-Oct 2020, Nov-Jan 2021). In addition, we included the total number of COVID-19 disease severity modulating co-morbidities (TOTALCMB), diabetes (type1, type2) (DM), obesity (OBESITY), hypertension (HTN), cardiovascular disease (CVD), pulmonary disease, chronic kidney disease (CKD), chronic liver disease, cancer (CANCER) and immune deficiency (IMMDF). Additionally, the model also included whether the patients were treated with the drug Remdesivir (CM\_RMDSVR) or Steroids (CM\_STERIODS) at baseline and how long they had been symptomatic from COVID-19 (SymOnSet). The R package "lme4" was used to fit the mixed linear model to each measurement and test for difference in antibody features depending on whether a patient received CCP or not. The  $p$  value from the likelihood ratio test and  $t$  value (normalized coefficients) associated with the variable represented two arms of the clinical trial, CP\_vs\_Control in full model, were visualized in a volcano plot using the ggplot function in R package 'ggplot2' (Version 3.3.5).

### Linear model to identify the percentage of explained variance

We built a linear model to identify the association of Nucleocapsid-related antibody features with clinical outcomes in CCP-treated and control individuals. The linear model used the same clinical characteristics involved in our previous models and N-related measurements from the second week (Day 8 and Day 15 measurements) of the clinical trial to predict the clinical outcomes as measured by the CSC. The details of the linear model are shown as follows:

$\text{CLINICAL\_SEVERITY\_SCORE} \sim 1 + \text{N\_C1q} + \text{N\_FCAR} + \text{N\_FCGR2AH} + \text{N\_FCGR2B} + \text{N\_FCGR3AV} + \text{N\_FCGR3B} + \text{N\_FCRN} + \text{N\_IgA1} + \text{N\_IgG1} + \text{N\_IgG2} + \text{N\_IgG3} + \text{N\_IgG4} + \text{N\_IgM} + \text{N\_ADCP} + \text{N\_ADNP} + \text{N\_107a\_ADNK} + \text{N\_IFNg\_ADNK} + \text{N\_MIP1b\_ADNK} + \text{AGE\_CAT} + \text{GENDER} + \text{RACE} + \text{ETHNICITY} + \text{POOL\_BLOOD} + \text{ENROLLQTR} + \text{TOTALCMB} + \text{DM} + \text{CVD} + \text{HTN} + \text{OBESITY} + \text{CKD} + \text{CANCER} + \text{IMMDF} + \text{CM\_RMDSVR} + \text{CM\_STERIODS} + \text{SymOnSet}$ .

Then, the percentage of explained variance in CSC attributed to each antibody feature was calculated by Sum of Square in ANOVA.

### **Unsupervised clustering to identifying the patterns in Day0**

Using all the measurements or the selected subset of measurements, the spearman correlation coefficients across the measurements were calculated to represent the sample-sample similarities. Then, we applied community detection method to the similarity matrix to identify the groups with more homogeneous immune profiles. First, we made a K-nearest neighbor graph based on similarity distance. Secondly, we calculated the adjacent matrix and identified the communities using the R package 'igraph'. Here, the parameter K was searched exhaustively from low number (2) to high number, in which all the samples were grouped into one cluster. The number of clusters was selected with the largest averaged silhouette values across all the clustering results.

To identify the measurements distinguished cluster four from the other clusters (Cluster 1,2, 3), we compared the samples inside the cluster four and those outside it using the wilcox-rank test implemented in the wilcoxauc function, in the presto R package. This process was repeated only with the 14 measurements that made up the CCP benefit signature to create Cluster A and B. The same clustering procedure described above was followed to determine cluster A and B.

To evaluate whether antibody levels or function was a more important determinant of response to CCP therapy, we created three linear models based on following measurements that most distinguished Cluster 4 from Cluster 1, 2, 3: 1) the 14 antibody titers, 2) the 14 antibody functions w/o IgG1 normalization, and 3) 14 antibody functions w/IgG1 normalization. These models were fitted and the percentage of explained variance was determined with the R package "lme4".

### **Discriminant analysis in Day60**

The log<sub>2</sub> Fold change of the average value per each measurement was calculated between CCP treatment arm and control arm. The p values were estimated by the permutation test through shuffling the arm labels. In detail, we randomly shuffled the arm labels and recalculated the log<sub>2</sub> Fold change of the mean values in the two groups for 1000 times and then the p values were estimated by the rank of the actual Fold change among the values of shuffled fold changes.

Then, the classification models were trained to distinguish control and treatment groups with a minimum set of measurements. We first applied LASSO feature selection and then trained partial least squares discriminant analysis (PLS-DA) classifier on the selected features as described above. The model performance was evaluated by 5-fold cross-validation. Finally, the network analysis was used to investigate the correlated features between selected features and non-selected features. The significant spearman correlation above the threshold of  $|r| > 0.3$ , were visualized within the networks.